Condition numbers of finite element methods on a class of anisotropic meshes ☆

Hengguang Li [a],*, Xun Lu [b]

[a] *Department of Mathematics, Wayne State University, Detroit, MI 48202, USA*
[b] *School of Mathematics and Computational Science, Xiangtan University, Hunan Province, Xiangtan 411105, PR China*

ABSTRACT

We study the behavior of the finite element condition numbers on a class of anisotropic meshes. These newly-developed mesh algorithms can produce numerical approximations with optimal convergence to isotropic and anisotropic singular solutions of elliptic boundary value problems in two- and three-dimensions. Despite the simplicity and fewer geometric constraints in implementation, these meshes can be highly anisotropic and do not maintain the maximum angle condition. We formulate a unified refinement principle and establish sharp estimates on the growth rate of the condition numbers of the stiffness matrix from these meshes. These results are important for effective applications of these meshes and for the design of fast numerical solvers. Numerical tests validate the theoretical analysis.

1. Introduction

Let $\Omega \subset \mathbb{R}^d$, $d = 2, 3$, be a bounded polytopal domain. Namely, Ω is a polygon ($d = 2$) or a polyhedron ($d = 3$). Consider the Poisson equation with the Dirichlet boundary condition as the model problem,

$$-\Delta u = f \quad \text{in} \quad \Omega, \qquad u = 0 \quad \text{on} \quad \partial\Omega. \tag{1}$$

The solution regularity of elliptic boundary value problems highly depends on the geometry of the domain. For example, even if the given data f is smooth, the solution of equation (1) may have singularities near the non-smooth points (vertices for $d = 2$, and vertices and edges for $d = 3$) on the boundary of the domain. These singularities can severely deteriorate the convergence of the numerical approximation. A popular approach is to increase the mesh density near the non-smooth points capturing the high-frequency components of the solution. For two-dimensional (2D) elliptic problems, this approach has led to mesh algorithms [1,8,10,31,34,36,41] that can recover the optimal convergence of finite element methods (FEMs) approximating singular solutions. These 2D elements vary much in size depending on their distance to the vertices, while they are isotropic and shape regular, which is consistent with the behavior of the 2D corner singularity.

The situation for three-dimensional (3D) problems is much more challenging. Both the vertices and the edges of the domain can give rise to singularities in the solution. The 3D vertex singularity is isotropic, carrying features similar to the

2D vertex singularity but in a higher dimension. The 3D edge singularity shows a distinctive character: it is anisotropic – singular in directions orthogonal to the edge and smoother in the edge direction. According to the aspect ratio of the element, the existing graded mesh algorithms for 3D singularities can be divided into two categories: isotropic and anisotropic. The *isotropic* meshes include most of the adaptive meshes from a-posteriori estimates [18,19,41] and the dyadic-partitioning meshes [2,22,35] based on a-priori analysis. These meshes are shape regular but the associated FEMs lose the optimal convergence when the edge singularity is strong or when high-order FEMs are used. The *anisotropic* mesh algorithms include the one in [1,3–5] that is based on the coordinate transformation from a quasi-uniform mesh, and the one in [9,11] that involves extra steps for prism refinements to maintain the angle condition of the simplex. Although the FEMs obtain the optimal convergence on both meshes, these algorithms are complicated to implement in general polyhedral domains, and do not result in well-structured (nested) finite element spaces. This is largely because these algorithms have geometric restrictions on simplexes to keep the maximum angle condition of the mesh. Recall that the maximum angle condition is often a rule of thumb to start with in developing numerical schemes, and the use of meshes without the maximum angle condition may lead to reduced convergence to functions in the Sobolev space. See for example the works of Babuška and Aziz [7] and of Křížek [26]. We also mention the works [6,20,21,23,28,37–39] where other relevant 2D and 3D anisotropic meshes were studied for various anisotropic problems.

Recently, a set of mesh algorithms were proposed in [10,29–34] for both 2D and 3D domains. These algorithms are simple, explicit, and applied to general polytopal domains. Based on reclusive refinements of the initial mesh, these meshes give rise to finite element solutions converging to the singular solution at the optimal convergence rate. These algorithms merely need a reasonable initial mesh of the domain, and the resulting meshes are conformal and similar in topology and data structure to the quasi-uniform mesh, and therefore can potentially improve practical computations solving singular problems. Such flexibility also means less control on the shape regularity. Existing finite element analysis is often built upon the assumption of an isotropic and shape regular mesh. However, these new meshes can be highly anisotropic and lose the maximum angle condition. Therefore, unconventional analytical and computational tools are needed for further developments and to broaden the application range of these methods.

We have two main tasks in this paper. 1. We formulate a refinement principle that will cover a wide range of 2D and 3D graded mesh algorithms in a unified frame work. This meshing principle is of interest itself, giving rise to not only the aforementioned 2D isotropic meshes [1,10,31] for corner singularities and the 3D anisotropic meshes [30,32,33], but also 2D anisotropic meshes for degenerate elliptic problems [29]. Due to the possible lack of the maximum angle condition, we shall hereafter refer to these meshes as no-maximum-angle-condition (NoMAC) meshes. 2. We study the condition numbers of FEMs on 2D and 3D NoMAC meshes. The conditioning of the numerical scheme is instructional in effective implementations of the algorithm, and in design of fast matrix solvers for the discrete system. Most of the existing conditioning estimates are for *shape regular* meshes. We here summarize some well-known results [12,15,40] that are relevant to this paper. On a shape regular mesh, let N be the dimension of the finite element space and let h_{min} be the smallest element size in the triangulation. Then, the condition number cond($\mathbf{A}_s$) of the scaled finite element stiffness matrix $\mathbf{A}_s$ satisfies

$$\begin{cases} \text{cond}(\mathbf{A}_s) \le CN(1 + |\log(Nh_{min}^2)|) & \text{(2D case)}, \\ \text{cond}(\mathbf{A}_s) \le CN^{2/3} & \text{(3D case)}. \end{cases} \tag{2}$$

In addition, we refer the readers to the following works on finite element condition numbers for other 3D graded meshes designed for vertex and edge singularities. For isotropic meshes near edges, see [2, Section 6]; for isotropic meshes near vertices and edges, see [5, Lemma 3.1 and Remark 3.2]; and for some anisotropic meshes, see [1, Section 4.3.3], where diagonal scaling was also discussed. All these meshes satisfy the maximum angle condition. For the anisotropic NoMAC meshes, we derive sharp estimates (Theorem 3.4 and Theorem 3.9) on the condition numbers in relation to the dimension of the discrete space and to the grading parameter of the algorithm. These new results are quite different from those on quasi-uniform meshes: the growth rates of the condition numbers in 2D are different for isotropic and anisotropic meshes; while for both isotropic and anisotropic meshes in 3D, there is a threshold value for the grading parameter, which determines whether the growth rate resembles the one on quasi-uniform meshes, or the growth rate is largely decided by the grading parameter. The main difficulty in the analysis lies in the anisotropic nature of the elements. The usual procedure in [12] cannot produce estimates that reflect the actual behavior of the condition number on NoMAC meshes. Our analysis relies on new observations on the anisotropic affine mapping for NoMAC meshes and a series of estimates in weighted function spaces.

The rest of the paper is organized as follows. In Section 2, we present the principle and algorithms for NoMAC meshes. Important properties and observations on these meshes will be discussed. In Section 3, we devise analysis for the condition number on 2D and 3D NoMAC meshes. Due to the nature of the mesh algorithm, estimates are first obtained in local regions of the domain, distinguished by their distance to different parts of the boundary. The main condition number estimates are summarized in Theorem 3.4 (2D) and in Theorem 3.9 (3D). We report numerical test results in Section 4 from various sample meshes to verify the theoretical prediction.

Throughout the text below, we adopt the bold notation for vectors and matrices. Let T be a triangle (resp. tetrahedron) with vertices a, b, c (resp. a, b, c, d). Then, we denote T by its vertices: $\triangle^3 abc$ for the triangle and $\triangle^4 abcd$ for the tetrahedron, where the sup-index implies the number of vertices for T. By $a \simeq b$, we mean there exists a constant $C > 0$ independent of a and b, such that $C^{-1}a \le b \le Ca$. In addition, by $A \subset B$, we mean A is a proper subset of B or $A = B$.

The generic constant $C > 0$ in our estimates may be different at different occurrences. It will depend on the computational domain, but not on the functions involved or the mesh level in the finite element algorithms.

2. The NoMAC mesh

2.1. The finite element method

Denote by $H^m(\Omega)$, $m \geq 0$, the Sobolev space that consists of functions whose ith derivatives are square integrable for $0 \leq i \leq m$. Let $L^2(\Omega) := H^0(\Omega)$. Recall that $H_0^1(\Omega) \subset H^1(\Omega)$ is the subspace consisting of functions with zero trace on the boundary $\partial\Omega$. The variational solution $u \in H_0^1(\Omega)$ of equation (1) satisfies

$$a(u, v) = \int_\Omega \nabla u \cdot \nabla v dx = \int_\Omega f v dx = (f, v), \quad \forall v \in H_0^1(\Omega). \tag{3}$$

Let $\mathcal{T}_n = \{T_\ell\}$ be a triangulation of Ω with triangles ($d = 2$) or tetrahedra ($d = 3$). It will become clear later that the index n represents the level of the mesh refinement. Let $S_n \subset H_0^1(\Omega)$ be the Lagrange finite element space of degree $k \geq 1$ associated with $\mathcal{T}_n$. Namely,

$$S_n = \{v \in C(\Omega), \ v|_T \in P_k, \text{ for any element } T \in \mathcal{T}_n\}, \tag{4}$$

where P_k is the space of polynomials of degree $\leq k$. Then, the finite element solution $u_n \in S_n$ for equation (1) is defined by

$$a(u_n, v_n) = (f, v_n), \quad \forall v_n \in S_n. \tag{5}$$

Denote by $N := \dim(S_n)$ the dimension of the finite element space. Let ϕ_i, $1 \leq i \leq N$, be the basis function associated to the ith node in $\mathcal{T}_n$. Then, the finite element equation (5) is equivalent to the linear system of equations

$$\mathbf{Au} = \mathbf{f}, \tag{6}$$

where for $1 \leq i, j \leq N$, $\mathbf{A}$ is the $N \times N$ stiffness matrix with entry $a_{ij} = a(\phi_i, \phi_j)$, the vector $\mathbf{f} = (f_1, f_2, \cdots, f_N)^T$ is defined by $f_i = (f, \phi_i)$, and the vector $\mathbf{u} = (u_1, u_2, \cdots, u_N)^T$ is the collection of the unknown coefficients in the representation of the finite element solution $u_n = \sum_{i=1}^N u_i \phi_i$.

Let $w \in S_n$ be a function in the finite element space (4) and let

$$\mathbf{w} = (w_1, w_2, \cdots, w_N)^T \tag{7}$$

be the associated vector such that $w = \sum_{\ell=1}^N w_\ell \phi_\ell$. Recall the l^2-norm of $\mathbf{w}$

$$\|\mathbf{w}\|_{l^2} = (\mathbf{w}^T \mathbf{w})^{1/2} = \Big(\sum_{1 \leq \ell \leq N} w_\ell^2 \Big)^{1/2}.$$

Note that by equations (3) and (5), $\mathbf{A}$ is a real symmetric positive definite matrix and all its eigenvalues are positive. Let

$$\lambda_{max} = \max_{\|\mathbf{w}\|_{l^2} \neq 0} \frac{\mathbf{w}^T \mathbf{Aw}}{\mathbf{w}^T \mathbf{w}}, \qquad \lambda_{min} = \min_{\|\mathbf{w}\|_{l^2} \neq 0} \frac{\mathbf{w}^T \mathbf{Aw}}{\mathbf{w}^T \mathbf{w}} \tag{8}$$

be the largest and the smallest eigenvalues, respectively. Then, the l^2-condition number cond($\mathbf{A}$) of the stiffness matrix is given by

$$\text{cond}(\mathbf{A}) = \lambda_{max}/\lambda_{min}. \tag{9}$$

It follows from a direct calculation that

$$\mathbf{w}^T \mathbf{Aw} = a(w, w) = \|\nabla w\|_{L^2(\Omega)}^2. \tag{10}$$

We shall study the condition number (9) on a class of anisotropic graded meshes.

2.2. The NoMAC mesh algorithms

We here present the algorithms that cover a class of graded meshes that appeared in [1,10,14,25,29,31,30,32,33]. These meshes can effectively improve the finite element approximation when the solution possesses singularities in 2D and 3D, especially from the non-smoothness of the computational domain. Unlike the conventional shape regular grids, these algorithms produce anisotropic no-maximum-angle-condition (NoMAC) meshes.

Let $\mathcal{V}$ (resp. $\mathcal{E}$) be the set of vertices (resp. the set of closed boundary edges) of the domain Ω. For each vertex $v \in \mathcal{V}$ and each edge $e \in \mathcal{E}$, we assign the associated grading parameter $\kappa_v \in (0, 0.5]$ and $\kappa_e \in (0, 0.5]$, respectively. Let $\mathcal{T}$ be a triangulation of Ω with triangles ($d = 2$) or tetrahedra ($d = 3$).
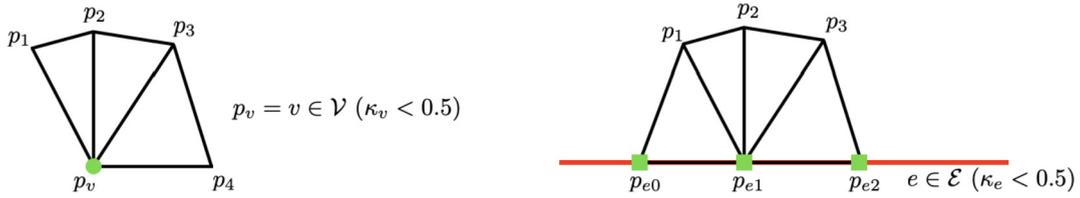
Fig. 1. Singular vertices and edges: a v-singular vertex $p_v = v \in \mathcal{V}$ with $\kappa_v < 0.5$ (left); e-singular vertices p_{e0}, p_{e1}, and p_{e2} on $e \in \mathcal{E}$ (red line segment) with $\kappa_e < 0.5$ (right). p_v is a singular vertex for all the edges $p_v p_i$, $1 \le i \le 4$. p_{e0} is a singular vertex for $p_{e0} p_1$, p_{e1} is a singular vertex for $p_{e1} p_i$, $1 \le i \le 3$, and p_{e2} is a singular vertex for $p_{e2} p_3$. $p_{e0} p_{e1}$ and $p_{e1} p_{e2}$ are singular edges. (For interpretation of the colors in the figure(s), the reader is referred to the web version of this article.)

Fig. 2. Refinement of an edge pq (left – right): no singular vertices (midpoint); p is a singular vertex ($|pr| = \kappa_p |pq|$, $\kappa_p < 0.5$).

Definition 2.1 *(Singular vertices and edges).* The singular vertices and singular edges are the special vertices and edges of the triangles or tetrahedra in $\mathcal{T}$ defined as follows. Let pq be a closed edge of an element $T \in \mathcal{T}$ with p and q as the endpoints. We define different singular sets based on the location of the edge pq. We say pq is a *singular edge* if $pq \subset e \in \mathcal{E}$ and $\kappa_e < 0.5$. Namely a singular edge in $\mathcal{T}$ lies on an edge e of the domain boundary for which the parameter $\kappa_e < 0.5$. We further describe two types of *singular vertices*. We call p a *v-singular vertex* if $p = v \in \mathcal{V}$ and $\kappa_v < 0.5$. In this case, p is a singular vertex for all the element edges connecting to p. We call p an *e-singular vertex* of pq if the following three conditions are satisfied: 1. p is not a v-singular vertex; 2. p lies on a singular edge that belongs to $e \in \mathcal{E}$ with $\kappa_e < 0.5$; 3. $pq \not\subset e$. In this case, p is a singular vertex for all the element edges intersecting e at p, but is not a singular vertex for the singular edges on e. See Fig. 1 for examples of the singular vertices and edges.

To simplify the presentation, we require that each element in $\mathcal{T}$ contains at most one singular edge and at most one v-singular vertex; and if it contains both, the v-singular vertex is an endpoint of the singular edge. Thus, each element edge in the triangulation has at most one singular vertex as an endpoint. Suppose p is a singular vertex of an edge pq in the triangulation. Then, we assign p a grading parameter κ_p as follows

$$\kappa_p := \begin{cases} \kappa_e, & \text{if } p \in e \in \mathcal{E} \text{ is an } e\text{-singular vertex,} \\ \min_{e \in \mathcal{E}_v} (\kappa_v, \kappa_e), & \text{if } p = v \in \mathcal{V} \text{ is an } v\text{-singular vertex,} \end{cases} \tag{11}$$

where $\mathcal{E}_v \subset \mathcal{E}$ is the set of edges that touch the vertex v.

The concept of singular vertices and edges shall be used to derive anisotropic mesh algorithms. In particular, the singular edge is useful to solve 2D anisotropic elliptic problems and 3D anisotropic edge singularities. See also Remark 2.5. According to Definition 2.1, each singular vertex p of an element edge is assigned a parameter $\kappa_p < 0.5$. Then, we describe the algorithm to produce new nodes on edges in the triangulation.

Algorithm 2.2 *(New nodes).* Let pq be an edge in the triangulation $\mathcal{T}$ with p and q as the endpoints. Then, in a graded refinement, a new node r on pq is produced according to the following conditions:

1. (Neither p or q is a singular vertex of pq.) We choose r as the midpoint ($|pr| = |qr|$).
2. (p is a singular vertex of pq.) We choose r such that $|pr| = \kappa_p |pq|$, where κ_p is defined in (11).

See Fig. 2 for an illustration.

Before presenting the NoMAC refinement algorithm, we note that based on the number of singular vertices and the number of singular edges in an element, we can classify the elements in $\mathcal{T}$ as follows.

Definition 2.3 *(Element types).* Given the conditions on the singular vertices and singular edges in Definition 2.1. Each element $T \in \mathcal{T}$ falls into one of the five categories.

1. o-element: $\bar{T}$ contains no singular vertex or singular edge.
2. v-element: $\bar{T}$ contains a v-singular vertex but no singular edge.
3. v_e-element: $\bar{T}$ contains an e-singular vertex but no singular edge.
4. e-element: $\bar{T}$ contains a singular edge but no v-singular vertex.
5. ev-element: $\bar{T}$ contains a v-singular vertex and a singular edge.

Now, we give the anisotropic mesh algorithm in 2D and 3D.
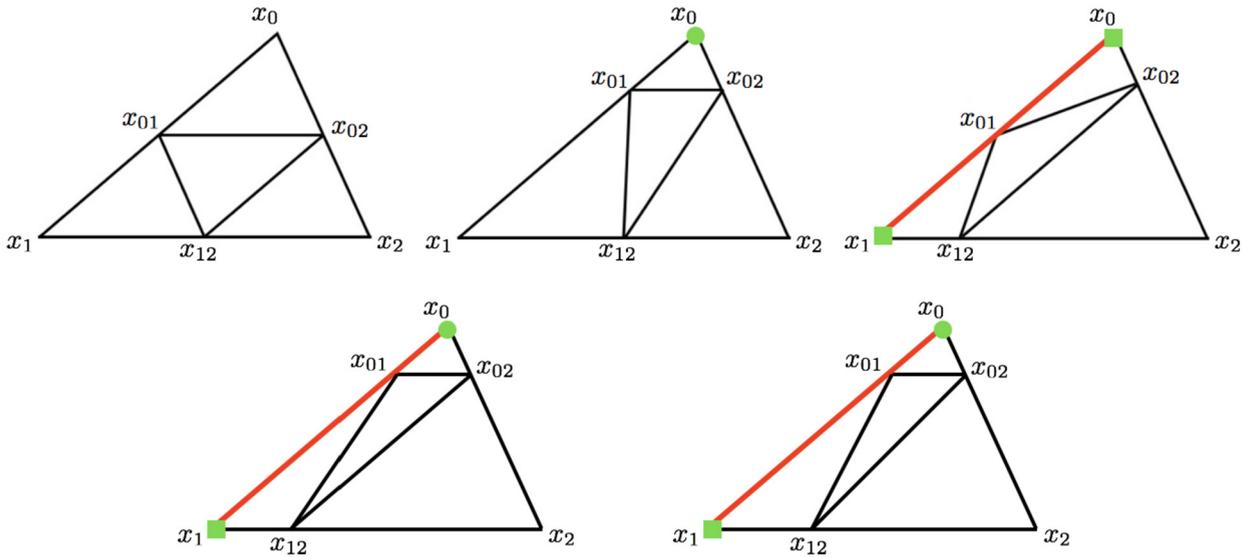
Fig. 3. Refinement of a triangle (green dot = v-singular vertex, green box = e-singular vertex, red line segment = singular edge). Top row (left – right): o-element, v-element, e-element. Bottom row (ev-elements, v-singular vertex $x_0 = v \in \mathcal{V}$ and singular edge $x_0x_1 \subset e \in \mathcal{E}$): $\kappa_e = \kappa_v$ (left); $\kappa_e > \kappa_v$ (right).
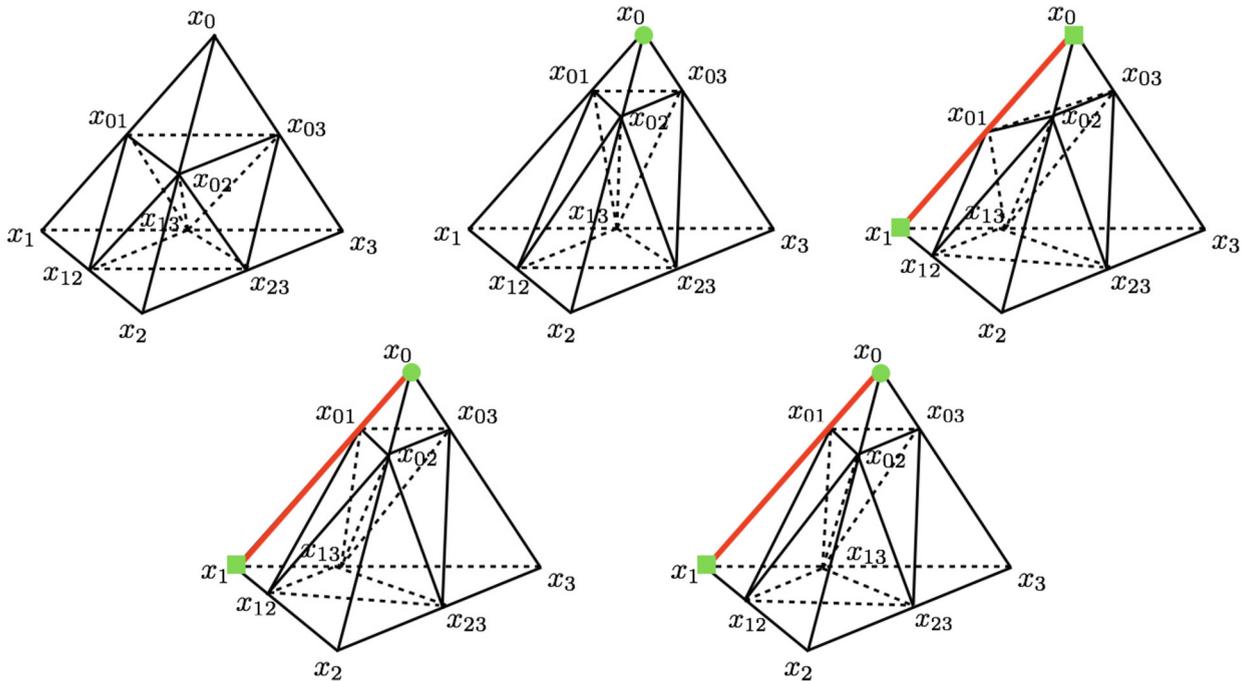
Fig. 4. Refinement of a tetrahedron (green dot = v-singular vertex, green box = e-singular vertex, red line segment = singular edge). Top row (left – right): o-element, v-element, e-element. Bottom row (ev-elements, v-singular vertex $x_0 = v \in \mathcal{V}$ and singular edge $x_0x_1 \subset e \in \mathcal{E}$): $\kappa_e = \kappa_v$ (left); $\kappa_e > \kappa_v$ (right).

Algorithm 2.4 (*NoMAC meshes*). Recall the triangulation $\mathcal{T}$ in Definition 2.1 and the grading parameter κ_p in (11) for each singular vertex p. Then, the graded refinement, denoted by $\kappa(\mathcal{T})$, proceeds as follows.

- Triangular Elements ($d = 2$). For each triangle $T = \triangle^3 x_0 x_1 x_2 \in \mathcal{T}$, a new node is generated on each edge based on Algorithm 2.2. Then, T is decomposed into four small triangles by connecting these new nodes (Fig. 3).
- Tetrahedral Elements ($d = 3$). For each tetrahedron $T = \triangle^4 x_0 x_1 x_2 x_3 \in \mathcal{T}$, a new node x_{kl} is generated on each edge $x_k x_l$, $0 \leq k < l \leq 3$, based on Algorithm 2.2. Connecting these new nodes x_{kl} on all the faces of T, we obtain four small tetrahedra and one octahedron. The octahedron then is cut into four tetrahedra using x_{13} as the common vertex. Therefore, after one refinement, we obtain eight sub-tetrahedra for each $T \in \mathcal{T}$ denoted by their vertices (Fig. 4):
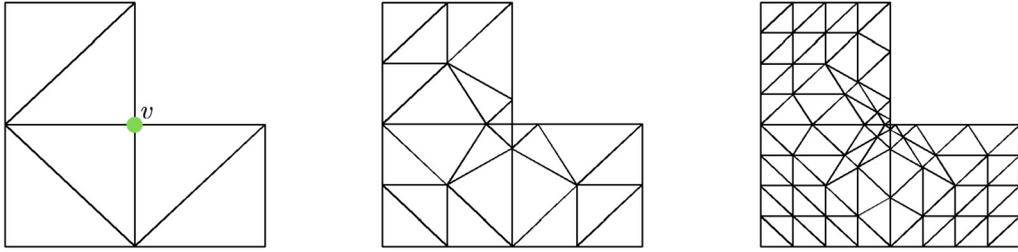
Fig. 5. 2D graded refinements toward a vertex v, ($\kappa_v = 0.2$).
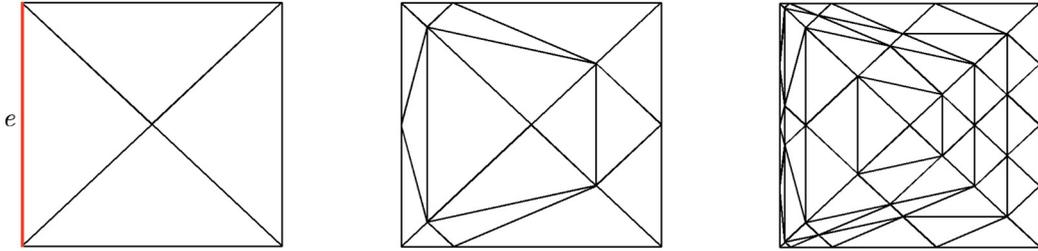
Fig. 6. 2D graded refinements toward an edge e, ($\kappa_e = 0.2$).
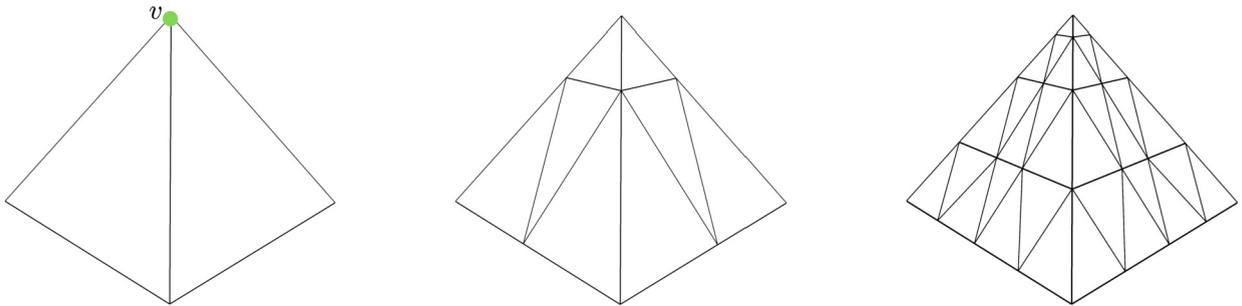
Fig. 7. 3D graded refinements toward a vertex v, ($\kappa_v = 0.25$).

$$\triangle^4 x_0 x_{01} x_{02} x_{03}, \ \triangle^4 x_{01} x_1 x_{12} x_{13}, \ \triangle^4 x_{02} x_{12} x_2 x_{23}, \ \triangle^4 x_{03} x_{13} x_{23} x_3,$$

$$\triangle^4 x_{01} x_{02} x_{03} x_{13}, \ \triangle^4 x_{01} x_{02} x_{12} x_{13}, \ \triangle^4 x_{02} x_{03} x_{13} x_{23}, \ \triangle^4 x_{02} x_{12} x_{13} x_{23}.$$

Given an initial mesh $\mathcal{T}_0$ satisfying the condition in Definition 2.1, the associated family of graded meshes $\{\mathcal{T}_n, \ n \geq 0\}$ is defined recursively $\mathcal{T}_n = \kappa(\mathcal{T}_{n-1})$. See Figs. 5 – Fig. 9 for example.

Remark 2.5. Recall the vertex singularity of equation (1) is isotropic, concentrating at the vertex of the domain; and the 3D edge singularity is anisotropic, singular in the direction perpendicular to the edge and smoother in the edge direction [17,24,30,32,33]. Thus, Algorithm 2.4 is based on a simple and intuitive idea: producing the new nodes closer to the singular point and consequently having new elements that are small in the direction of the singularity. Note that a v-singular vertex is a singular node for all the connecting edges; while an e-singular vertex is a singular node only for non-singular edges. Algorithm 2.4 covers a variety of graded meshes in the literature. It has shown its effectiveness in approximating 2D corner singularities [1,10,31,34], anisotropic degenerate elliptic operators [29], and solving 3D elliptic problems with vertex and edges singularities [30,32,33]. The regularity of the underlying solution in general plays an important role in deciding the singular vertices and edges and the associated grading parameters κ_e and κ_v in order to achieve the optimal convergence in the numerical solution. Compared with existing meshes, this new mesh enjoys advantages in practical computing for being explicit, and having fewer geometric constraints. However, Algorithm 2.4 can lead to meshes without the maximum angle condition, especially when there are singular edges (Figs. 6, 8, and 9). This makes the analysis for this algorithm both technical and interesting.
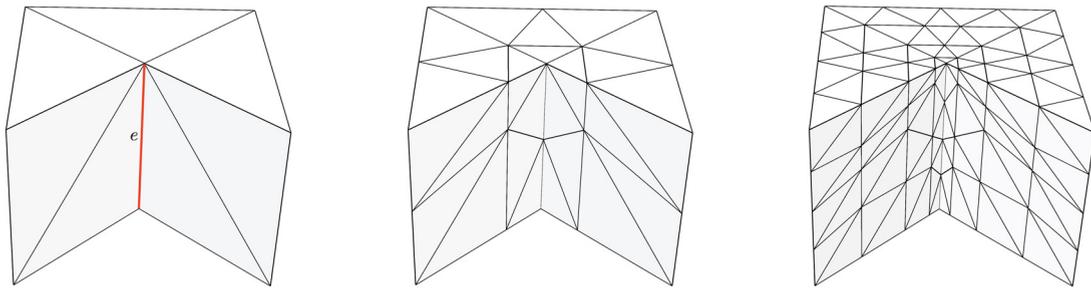
Fig. 8. 3D graded refinements toward an edge e, ($\kappa_e = 0.3$).
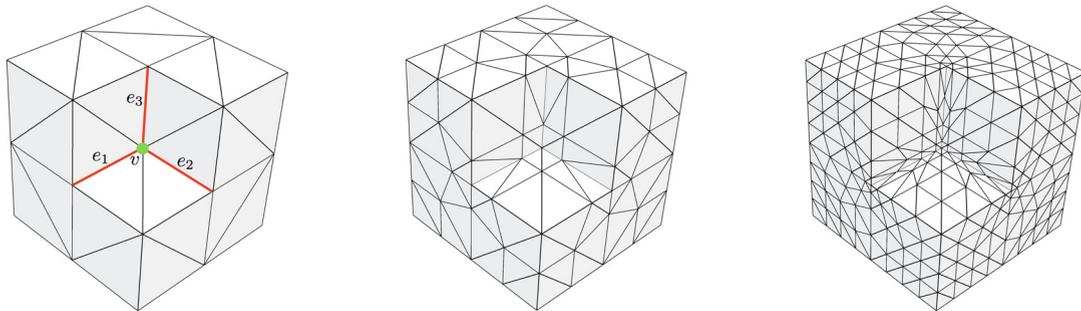
Fig. 9. 3D graded refinements toward a vertex v and its adjacent edges, ($\kappa_v = \kappa_{e_i} = 0.3$, $1 \leq i \leq 3$).

2.3. Mesh layers and affine mappings

We here derive properties of the NoMAC mesh that will be useful for the analysis. Based on the distance to the vertices and edges of the domain, we first define different layers of the mesh.

Definition 2.6 (*Mesh layers in initial v- or v_e-elements*). Let $T_{(0)} \in \mathcal{T}_0$ be an initial v- or v_e-element. Let $T_{(i)} \subset T_{(0)}$ be the element in $\mathcal{T}_i$, $0 \leq i \leq n$, that is attached to the singular vertex of $T_{(0)}$. For $0 \leq i < n$, we define the ith mesh layer of $\mathcal{T}_n$ on $T_{(0)}$ to be the region $L_{v,i} := T_{(i)} \setminus T_{(i+1)}$; and for $i = n$, the nth layer is $L_{v,n} := T_{(n)}$.

Remark 2.7. For the 2D v-element $T_{(0)} = \triangle^3 x_0 x_1 x_2$ in Fig. 3, $L_{v,0}$ is the trapezoid $x_1 x_2 x_{02} x_{01}$. For the 3D v-element $T_{(0)} = \triangle^4 x_0 x_1 x_2 x_3$ in Fig. 4, $L_{v,0}$ is the pentahedron $x_{01} x_{02} x_{03} x_1 x_2 x_3$. In both cases (trapezoid and pentahedron) and in the text below, we denote a polytope by its vertices. Let κ_p be the grading parameter associated with the singular vertex of $T_{(0)}$. According to Algorithm 2.4, the elements of $\mathcal{T}_n$ in the layer $L_{v,i}$ are isotropic and shape regular with mesh size $O(2^{i-n} \kappa_p^i)$.

Definition 2.8 (*Mesh layers in initial e-elements*). Let $T_{(0)} \in \mathcal{T}_0$ be an initial e-element. Let U_i be the union of elements in $\mathcal{T}_i$, $0 \leq i \leq n$, that touch the singular edge of $T_{(0)}$. For $0 \leq i < n$, we define the ith mesh layer of $\mathcal{T}_n$ on $T_{(0)}$ to be the region $L_{e,i} := U_i \setminus U_{i+1}$; and for $i = n$, the nth layer is $L_{e,n} := U_n$.

Remark 2.9. For the 2D e-element $T_{(0)} = \triangle^3 x_0 x_1 x_2$ in Fig. 3, $L_{e,0}$ is the trapezoid $x_0 x_1 x_{12} x_{02}$. For the 3D e-element $T_{(0)} = \triangle^4 x_0 x_1 x_2 x_3$ in Fig. 4, $L_{e,0}$ is the pentahedron $x_0 x_{02} x_{03} x_1 x_{12} x_{13}$. According to Algorithm 2.4, the elements of $\mathcal{T}_n$ in the layer $L_{e,i}$ are anisotropic, whose largest angle in the face converges to π as $n \to \infty$.

Definition 2.10 (*Mesh layers in initial ev-elements*). Let $T_{(0)} \in \mathcal{T}_0$ be an initial ev-element. Let $T_{(i)} \subset T_{(0)}$ be the ev-element in $\mathcal{T}_i$, $0 \leq i \leq n$, that is attached to the singular vertex and the singular edge of $T_{(0)}$. For $0 \leq i < n$, we define the ith mesh layer of $\mathcal{T}_n$ on $T_{(0)}$ to be the region $L_{ev,i} := T_{(i)} \setminus T_{(i+1)}$; and for $i = n$, the nth layer is $L_{ev,n} := T_{(n)}$.

Remark 2.11. For the 2D ev-element $T_{(0)} = \triangle^3 x_0 x_1 x_2$ in Fig. 3, $L_{ev,0}$ is the trapezoid $x_1 x_2 x_{02} x_{01}$. For the 3D ev-element $T_{(0)} = \triangle^4 x_0 x_1 x_2 x_3$ in Fig. 4, $L_{ev,0}$ is the pentahedron $x_{01} x_{02} x_{03} x_1 x_2 x_3$. Although the mesh layers in initial ev-elements follow a similar construction as those in initial v- or v_e-elements (Definition 2.6), the elements of $\mathcal{T}_n$ in the layer $L_{ev,i}$ are anisotropic whose largest angle in the face can be arbitrarily close to π. One can compare this to the statements in Remarks 2.7 and 2.9.

Based on Algorithm 2.4, the refinement of an element T can result in small elements of different types. For example, for $d = 2$, after one refinement, an e-element T is decomposed into four small elements: two e-elements, one v_e-element, and

one o-element. For $d = 3$, after one refinement, an e-element T is decomposed into eight small elements: two e-elements, two v_e-elements, and four o-elements. Nevertheless, in a refinement, we call T the *parent element* of the small elements, and call each small element the *child element* of T.

Recall the mesh layers of the triangulation $\mathcal{T}_n$ in Definitions 2.6, 2.8, and 2.10. We now construct affine mappings between a region in each layer and a reference region whose shape may depend on an initial element in $\mathcal{T}_0$ but not on n.

Proposition 2.12 (*Affine mappings on initial v-, v_e-, and ev-elements*). *Let $T_{(0)} \in \mathcal{T}_0$ be a v-, v_e-, or ev-element in the initial triangulation. Let κ_p be the grading parameter associated with the singular vertex. We use a local coordinate system such that the singular vertex of $T_{(0)}$ is the origin. Define two mappings*

$$\mathbf{B}_{v,i}^{(3)} = \begin{pmatrix} \kappa_p^{-i} & 0 & 0 \\ 0 & \kappa_p^{-i} & 0 \\ 0 & 0 & \kappa_p^{-i} \end{pmatrix}, \quad d = 3 \quad \text{and} \quad \mathbf{B}_{v,i}^{(2)} = \begin{pmatrix} \kappa_p^{-i} & 0 \\ 0 & \kappa_p^{-i} \end{pmatrix}, \quad d = 2. \tag{12}$$

Then, for $d = 3$ and $1 \le i < n$, $\mathbf{B}_{v,i}^{(3)}$ is a bijection between the ith layer $L_{v,i}$ (or $L_{ev,i}$ depending on the element type of $T_{(0)}$) and the first layer $L_{v,0}$ (or $L_{ev,0}$) on $T_{(0)}$; for $i = n$, $\mathbf{B}_{v,n}^{(3)}$ is a bijection between $L_{v,n}$ (or $L_{ev,n}$) and $T_{(0)}$. The dilation $\mathbf{B}_{v,i}^{(2)}$ is the 2D analogue of $\mathbf{B}_{v,i}^{(3)}$. Namely, $\mathbf{B}_{v,i}^{(2)}$ maps the 2D ith layer to the first layer ($0 \le i < n$) or to the initial element $T_{(0)}$ ($i = n$).

Proof. See Definition 4.2 in [30] for the proof when $d = 3$. The 2D case is also a direct consequence of Algorithms 2.2 and 2.4. □

Proposition 2.13 (*Affine mappings on initial e-elements*). *Let $T_{(0)} \in \mathcal{T}_0$ be an e-element in the initial triangulation and let κ_e be the grading parameter associated with the singular edge. Let $T'_{(i+1)} \in \mathcal{T}_{i+1}$ be an element, such that $T'_{(i+1)} \subset L_{e,i} \subset T_{(0)}$, $0 \le i < n$; and $T'_{(n)} \subset L_{e,n} \subset T_{(0)}$ if $i = n$. Then, we have two cases to consider. (I) $T'_{(i+1)}$ is a child element of an e-element $T_{(i)} \in \mathcal{T}_i$ for $i < n$ or $T'_{(n)}$ is an e-element for $i = n$. Then, we can choose a proper local coordinate system (where the singular edge is on the y-axis (2D) or on the z-axis (3D)) and a reference element $\hat{T}$ whose geometry only depends on the initial element $T_{(0)}$, such that*

$$\mathbf{B}_{e,i}^{(3)} = \begin{pmatrix} \kappa_e^{-i} & 0 & 0 \\ 0 & \kappa_e^{-i} & 0 \\ b_1 \kappa_e^{-i} & b_2 \kappa_e^{-i} & 2^i \end{pmatrix}, \quad d = 3 \quad \text{and} \quad \mathbf{B}_{e,i}^{(2)} = \begin{pmatrix} \kappa_e^{-i} & 0 \\ b_3 \kappa_e^{-i} & 2^i \end{pmatrix}, \quad d = 2 \tag{13}$$

are bijections from $T'_{(i+1)}$ to $\hat{T}$ in 3D and 2D, respectively. (II) $T'_{(i+1)}$ is a child element of a v_e-element $T_{(i)} \in \mathcal{T}_i$ for $i < n$ or $T'_{(n)}$ is a v_e-element for $i = n$. Let $T_{(k)} \in \mathcal{T}_k$, $1 \le k \le i$, be the v_e-element, such that $T_{(i)} \subset T_{(k)}$ for $i < n$ or $T'_{(n)} \subset T_{(k)}$ for $i = n$, and $T_{(k)}$'s parent element $T_{(k-1)} \in \mathcal{T}_{k-1}$ is an e-element. Then, we can choose a proper local coordinate system and a reference element $\hat{T}$ whose geometry only depends on the initial element $T_{(0)}$, such that the transformations

$$\mathbf{B}_{i,k}^{(3)} = \begin{pmatrix} \kappa_e^{1-i} & 0 & 0 \\ 0 & \kappa_e^{1-i} & 0 \\ b_1 \kappa_e^{1-i} & b_2 \kappa_e^{1-i} & 2^{k-1}\kappa_e^{k-i} \end{pmatrix}, \quad d = 3 \quad \text{and} \quad \mathbf{B}_{i,k}^{(2)} = \begin{pmatrix} \kappa_e^{1-i} & 0 \\ b_3 \kappa_e^{1-i} & 2^{k-1}\kappa_e^{k-i} \end{pmatrix}, \quad d = 2 \tag{14}$$

map $T'_{(i+1)}$ to $\hat{T}$ for $i < n$ and map $T'_{(n)}$ to $\hat{T}$ for $i = n$ in 3D and 2D, respectively. In both cases (I) and (II), $|b_1|, |b_2|, |b_3| \le C_0$, for $C_0 > 0$ depending on $T_{(0)}$ but not on i or k.

Proof. When $d = 3$, the statements for $\mathbf{B}_{e,i}^{(3)}$ and $\mathbf{B}_{i,k}^{(3)}$ follow from Lemma 4.15 in [30]. As revealed in Lemmas 4.13 and 4.14 of [30], the parameters b_1 and b_2 can be different for different tetrahedra, but they are uniformly bounded by a constant that depends on the initial tetrahedron $T_{(0)}$. When $d = 2$, the statements for $\mathbf{B}_{e,i}^{(2)}$ and $\mathbf{B}_{i,k}^{(2)}$ hold since the triangles involved can be regarded as triangles on the faces of the tetrahedra $T'_{(i+1)}$ and $\hat{T}$ in 3D. The mappings $\mathbf{B}_{e,i}^{(2)}$ and $\mathbf{B}_{i,k}^{(2)}$ are the restrictions of $\mathbf{B}_{e,i}^{(3)}$ and $\mathbf{B}_{i,k}^{(3)}$ on these faces. □

3. The conditioning on NoMAC meshes

In this section, we study the condition numbers (9) of the finite element method on the NoMAC mesh. Let $\mathcal{T}_n$ be the NoMAC mesh obtained after n consecutive refinements (Algorithm 2.4) from an initial triangulation $\mathcal{T}_0$. Throughout this section, we adopt the following notation. Let $w \in S_n$ and $\mathbf{w}$ be the function in the finite element space and its vector representation (7), respectively. For each element T, we shall specify a reference element $\hat{T}$ and an affine mapping $\mathbf{K} : T \to \hat{T}$, such that for any $(x, y) \in T$ ($d = 2$) or $(x, y, z) \in T$ ($d = 3$), $(\hat{x}, \hat{y}) := \mathbf{K}(x, y) \in \hat{T}$ ($d = 2$) or $(\hat{x}, \hat{y}, \hat{z}) := \mathbf{K}(x, y, z) \in \hat{T}$ ($d = 3$). In addition, for any function v on T, we define the function $\hat{v}(\hat{x}, \hat{y}) := v(x, y)$ ($d = 2$) or $\hat{v}(\hat{x}, \hat{y}, \hat{z}) := v(x, y, z)$ ($d = 3$) on $\hat{T}$.

Recall the types of elements in Definition 2.3. Denote by $D_o \subset \Omega$ the region covered by initial o-elements in $\mathcal{T}_0$. Similarly, we define D_v, D_{v_e}, D_e, and D_{ev} to be the regions covered by the corresponding initial elements in $\mathcal{T}_0$ whose type is indicated via the index of the region.

3.1. The 2D case

For the triangular mesh $\mathcal{T}_n$, we first have the following estimates on sub-regions of Ω excluding the singular edges.

Lemma 3.1. *Let $T \in \mathcal{T}_n$ be a triangle. Let I_o be the set of indices of the nodes in $\mathcal{T}_n$ that belong to $\bar{D}_o$. Similarly, let I_v and I_{v_e} be the sets of indices of the nodes in $\mathcal{T}_n$ that belong to $\bar{D}_v$ and $\bar{D}_{v_e}$, respectively. Then, we have*

$$\sum_{T \subset D_o \cup D_v \cup D_{v_e}} \|\nabla w\|_{L^2(T)}^2 \leq C \sum_{\ell \in I_o \cup I_v \cup I_{v_e}} w_\ell^2, \tag{15}$$

$$\sum_{\ell \in I_o} w_\ell^2 \simeq C 2^{2n} \sum_{T \subset D_o} \|w\|_{L^2(T)}^2. \tag{16}$$

In addition, for $T \subset D_v \cup D_{v_e}$, suppose T is in the ith mesh layer $L_{v,i}$ (Definition 2.6) on an initial element, with κ_p as the grading parameter for the singular vertex. Let I_T be the set of indices of the nodes in $\bar{T}$. Then, we have

$$\sum_{\ell \in I_T} w_\ell^2 \leq C 2^{2(n-i)} \kappa_p^{-2i} \|w\|_{L^2(T)}^2. \tag{17}$$

In (15) – (17), the constant C does not depend on i or n.

Proof. We consider different cases based on the location of the triangle involved.

Note that from Algorithms 2.2 and 2.4, the mesh on D_o is quasi-uniform with mesh size $O(2^{-n})$, since the refinement is based on the usual midpoint decomposition of a triangle. For $\mathcal{T}_n \ni T \subset D_o$, let $\hat{T} = T_{(0)}$ be the reference triangle, where $T_{(0)} \in \mathcal{T}_0$ is the initial triangle containing T. Let $\mathbf{K} : T \to \hat{T}$ be the standard affine mapping [15,16]. Note that the finite element space defined on the reference element $\hat{T}$ is finite dimensional and therefore any two norms are equivalent. We shall use this property multiple times in the paper and will refer to it as the norm equivalence in finite-dimensional spaces. Then, by the scaling argument and the norm equivalence in finite-dimensional spaces, we obtain

$$\sum_{T \subset D_o} \|\nabla w\|_{L^2(T)}^2 = \sum_{T \subset D_o} \int_T (\partial_x w)^2 + (\partial_y w)^2 dx dy$$
$$\leq C \sum_{T \subset D_o} \int_{\hat{T}} (\partial_{\hat{x}} \hat{w})^2 + (\partial_{\hat{y}} \hat{w})^2 d\hat{x} d\hat{y} \leq C \sum_{T \subset D_o} \|\hat{w}\|_{L^\infty(\hat{T})}^2 \leq C \sum_{\ell \in I_o} w_\ell^2. \tag{18}$$

Similarly, by the scaling argument and the norm equivalence in finite-dimensional spaces, we have

$$\sum_{T \subset D_o} \|w\|_{L^2(T)}^2 = \sum_{T \subset D_o} \int_T w^2 dx dy = 2^{-2n} \sum_{T \subset D_o} \int_{\hat{T}} \hat{w}^2 d\hat{x} d\hat{y}$$
$$\geq C 2^{-2n} \sum_{T \subset D_o} \|\hat{w}\|_{L^\infty(\hat{T})}^2 \geq C 2^{-2n} \sum_{\ell \in I_o} w_\ell^2. \tag{19}$$

For a triangle $T \in \mathcal{T}_n$ in D_v or in D_{v_e}, suppose T is in the ith layer of an initial triangle $T_{(0)}$. As in Definition 2.6, let $T_{(i)} \subset T_{(0)}$ be the element in $\mathcal{T}_i$ ($0 \leq i \leq n$) that touches the singular vertex of $T_{(0)}$. Then, if $i = n$, we have $T = T_{(n)}$; if $i < n$, we have $T \subset T'_{(i+1)} \subset T_{(i)}$, where $T'_{(i+1)} \in \mathcal{T}_{i+1}$ is an o-element. Based on Algorithm 2.4, if $i < n$, T is generated after $n - i - 1$ midpoint refinements of $T'_{(i+1)}$. Recall from Proposition 2.12 that $\mathbf{B}_{v,i}^{(2)}$ maps $T_{(i)}$ to $\hat{T} := T_{(0)}$. Then, the mapping $\mathbf{K} : T \to \hat{T}$ satisfies for $(x, y) \in T$ and $(\hat{x}, \hat{y}) = \mathbf{K}(x, y) \in \hat{T}$,

$$(\partial_x w)^2 + (\partial_y w)^2 \leq C 2^{2(n-i)} \kappa_p^{-2i} \big((\partial_{\hat{x}} \hat{w})^2 + (\partial_{\hat{y}} \hat{w})^2 \big) \quad \text{and} \quad dx dy \simeq 2^{2(i-n)} \kappa_p^{2i} d\hat{x} d\hat{y}. \tag{20}$$

Therefore, by (20) and the norm equivalence in finite-dimensional spaces, we have

$$\sum_{T \subset D_v \cup D_{v_e}} \|\nabla w\|_{L^2(T)}^2 = \sum_{T \subset D_v \cup D_{v_e}} \int_T (\partial_x w)^2 + (\partial_y w)^2 dx dy$$

$$\leq C \sum_{T \subset D_v \cup D_{v_e}} \int_{\hat{T}} (\partial_{\hat{x}} \hat{w})^2 + (\partial_{\hat{y}} \hat{w})^2 d\hat{x} d\hat{y} \leq C \sum_{T \subset D_v \cup D_{v_e}} \|\hat{w}\|^2_{L^\infty(\hat{T})}$$

$$\leq C \sum_{\ell \in I_v \cup I_{e_v}} w_\ell^2. \tag{21}$$

Meanwhile, using (20) and the norm equivalence in finite-dimensional spaces, we have

$$\|w\|^2_{L^2(T)} = \int_T w^2 dxdy \simeq 2^{2(i-n)} \kappa_p^{2i} \int_{\hat{T}} \hat{w}^2 d\hat{x} d\hat{y}$$

$$\geq C 2^{2(i-n)} \kappa_p^{2i} \|\hat{w}\|^2_{L^\infty(\hat{T})} \geq C 2^{2(i-n)} \kappa_p^{2i} \sum_{\ell \in I_T} w_\ell^2. \tag{22}$$

Hence, we have proved the estimate (15) by combining (18) and (21). The estimates (16) and (17) are due to (19) and (22), respectively. □

Now, we derive useful estimates in regions close to singular edges.

Lemma 3.2. *Let $T \in \mathcal{T}_n$ be an triangle in D_e. Suppose T is in the ith mesh layer $L_{e,i}$ (Definition 2.8) of an initial e-element $T_{(0)} \in \mathcal{T}_0$, with κ_e as the grading parameter for the singular edge. Let I_T be the set of indices of the nodes in $\bar{T}$. Then, we have*

$$\|\nabla w\|^2_{L^2(T)} \leq C (2\kappa_e)^{-n} \sum_{\ell \in I_T} w_\ell^2, \tag{23}$$

$$\sum_{\ell \in I_T} w_\ell^2 \leq C 2^{2(n-i)} \kappa_e^{-2i} \|w\|^2_{L^2(T)}, \tag{24}$$

where C depends on $T_{(0)}$ but not on i or n.

Proof. Let $T_{(i)} \in \mathcal{T}_i$ be the triangle such that $T \subset T_{(i)}$. Then, according to Definition 2.8, $T_{(i)}$ is either an e-element or a v_e-element. Based on Algorithm 2.4, if $i = n$, we have $T = T_{(n)}$. If $i < n$, we have $T \subset T'_{(i+1)} \subset T_{(i)}$, where $T'_{(i+1)} \in \mathcal{T}_{i+1}$ is an o-element, and T is generated after $n - i - 1$ midpoint refinements of $T'_{(i+1)}$.

Case I. $T_{(i)}$ is an e-element in $\mathcal{T}_i$ ($0 \leq i \leq n$). According to the arguments above and Proposition 2.13, $\mathbf{B}_{e,i}^{(2)}$ maps $T'_{(i+1)}$ ($i < n$) or $T_{(n)}$ ($i = n$) to a reference triangle $\hat{T}$ whose geometry only depends on $T_{(0)}$. Then, the mapping $\mathbf{K} : T \to \hat{T}$ satisfies for $(x, y) \in T$ and $(\hat{x}, \hat{y}) \in \hat{T}$,

$$(\partial_x w)^2 + (\partial_y w)^2 \leq C 2^{2(n-i)} \kappa_e^{-2i} \left((\partial_{\hat{x}} \hat{w})^2 + (\partial_{\hat{y}} \hat{w})^2\right) \quad \text{and} \quad dxdy \simeq (2\kappa_e)^i 2^{-2n} d\hat{x} d\hat{y}.$$

Then, by the norm equivalence in finite-dimensional spaces, we have

$$\|\nabla w\|^2_{L^2(T)} \leq C \int_{\hat{T}} 2^{2n} (2\kappa_e)^{-2i} \left((\partial_{\hat{x}} \hat{w})^2 + (\partial_{\hat{y}} \hat{w})^2\right) 2^{i-2n} \kappa_e^i d\hat{x} d\hat{y}$$

$$\leq C (2\kappa_e)^{-i} \|\hat{w}\|^2_{L^\infty(\hat{T})} \leq C (2\kappa_e)^{-i} \sum_{\ell \in I_T} w_\ell^2. \tag{25}$$

Similarly, we have

$$\|w\|^2_{L^2(T)} = \int_T w^2 dxdy \simeq 2^{-2n} (2\kappa_e)^i \int_{\hat{T}} \hat{w}^2 d\hat{x} d\hat{y}$$

$$\geq C 2^{-2n} (2\kappa_e)^i \|\hat{w}\|^2_{L^\infty(\hat{T})} \geq C 2^{-2n} (2\kappa_e)^i \sum_{\ell \in I_T} w_\ell^2. \tag{26}$$

Case II. $T_{(i)}$ is a v_e-element in $\mathcal{T}_i$ ($0 \leq i \leq n$). Let $T_{(k)} \in \mathcal{T}_k$, $1 \leq k \leq i$, be the v_e-element, such that $T_{(i)} \subset T_{(k)}$ and $T_{(k)}$'s parent element $T_{(k-1)} \in \mathcal{T}_{k-1}$ is an e-element. Then, according to Proposition 2.13, $\mathbf{B}_{i,k}^{(2)}$ maps $T'_{(i+1)}$ ($i < n$) or $T_{(n)}$ ($i = n$) to a reference triangle $\hat{T}$ whose geometry only depends on $T_{(0)}$. Then, the mapping $\mathbf{K} : T \to \hat{T}$ satisfies for $(x, y) \in T$ and $(\hat{x}, \hat{y}) \in \hat{T}$,

$$(\partial_x w)^2 + (\partial_y w)^2 \leq C 2^{2(n-i)} \kappa_e^{-2i} \left((\partial_{\hat{x}} \hat{w})^2 + (\partial_{\hat{y}} \hat{w})^2\right) \quad \text{and} \quad dxdy \simeq (2\kappa_e)^{2i-k} 2^{-2n} d\hat{x} d\hat{y}.$$

Then, by the norm equivalence in finite-dimensional spaces, we obtain

$$\|\nabla w\|^2_{L^2(T)} \le C \int_{\hat{T}} 2^{2n-2i} \kappa_e^{-2i} \big((\partial_{\hat{x}} \hat{w})^2 + (\partial_{\hat{y}} \hat{w})^2\big) 2^{-2n} (2\kappa_e)^{2i-k} d\hat{x} d\hat{y}$$

$$\le C(2\kappa_e)^{-k} \|\hat{w}\|^2_{L^\infty(\hat{T})} \le C(2\kappa_e)^{-k} \sum_{\ell \in I_T} w_\ell^2. \tag{27}$$

Similarly, we have

$$\|w\|^2_{L^2(T)} = \int_T w^2 dx dy \simeq (2\kappa_e)^{2i-k} 2^{-2n} \int_{\hat{T}} \hat{w}^2 d\hat{x} d\hat{y}$$

$$\ge C(2\kappa_e)^{2i-k} 2^{-2n} \|\hat{w}\|^2_{L^\infty(\hat{T})} \ge C(2\kappa_e)^{2i-k} 2^{-2n} \sum_{\ell \in I_T} w_\ell^2. \tag{28}$$

Recall $k \le i \le n$ and $\kappa_e < 0.5$. Then, we obtain (23) by summing up the estimates (25) and (27) over all $T \subset D_e$. The estimate (24) is due to (26) and (28). □

Then, we give some useful estimates on regions close to both singular vertices and singular edges.

Lemma 3.3. *Let $T \in \mathcal{T}_n$ be a triangle in D_{ev}. Let I_{ev} be the set of indices of the nodes in $\mathcal{T}_n$ that belong to $\bar{D}_{ev}$. Suppose T is in the ith mesh layer (Definition 2.10) of an initial ev-element, with κ_p and κ_e as the grading parameter for the singular vertex and for the singular edge, respectively. Then, we have*

$$\sum_{T \subset D_{ev}} \|\nabla w\|^2_{L^2(T)} \le C(2\kappa_e)^{-n} \sum_{\ell \in I_{ev}} w_\ell^2. \tag{29}$$

In addition, let I_T be the set of indices of the nodes in $\bar{T}$. For $i < n$, let $T'_{(i+1)} \in \mathcal{T}_{i+1}$ be the triangle that contains T. Note that $T'_{(i+1)}$ can be either an o-, v_e-, or e-element. If $T'_{(i+1)}$ is an o-element or if $i = n$, we have

$$\sum_{\ell \in I_T} w_\ell^2 \le C 2^{2(n-i)} \kappa_p^{-2i} \|w\|^2_{L^2(T)}. \tag{30}$$

If $T'_{(i+1)}$ $(i < n)$ is a v_e- or e-element, suppose T is in the kth $(k < n - i)$ layer (Definitions 2.6 and 2.8) of the graded triangulation on $T'_{(i+1)}$ toward the singular vertex or toward the singular edge. Then, we have

$$\sum_{\ell \in I_T} w_\ell^2 \le C 2^{2(n-i-k)} \kappa_p^{-2i} \kappa_e^{-2k} \|w\|^2_{L^2(T)}. \tag{31}$$

Proof. For a triangle T in D_{ev}, suppose $T \subset T_{(0)}$, where $T_{(0)}$ is an initial ev-element in $\mathcal{T}_0$. Therefore, T is either in the ith mesh layer $L_{ev,i}$ if $i < n$ and $T \subset T'_{(i+1)}$ for some $T'_{(i+1)} \in \mathcal{T}_{i+1}$; or $T = T_{(n)} \subset L_{ev,n}$.

We first consider the case when $i = n$, namely $T = T_{(n)}$. Then, the dilation $\mathbf{B}^{(2)}_{v,n}$ in (12) maps T to $\hat{T} = T_{(0)}$. Using the same scaling argument (20) as in Lemma 3.1, we obtain

$$\|\nabla w\|^2_{L^2(T)} \le C \sum_{\ell \in I_T} w_\ell^2. \tag{32}$$

In addition, by the scaling argument (20) and the norm equivalence in finite-dimensional spaces, we have

$$\|w\|^2_{L^2(T)} = \int_T w^2 dx dy \ge C \kappa_p^{2n} \int_{\hat{T}} \hat{w}^2 d\hat{x} d\hat{y}$$

$$\ge C \kappa_p^{2n} \|\hat{w}\|^2_{L^\infty(\hat{T})} \ge C \kappa_p^{2n} \sum_{\ell \in I_T} w_\ell^2. \tag{33}$$

We now consider the case when $i < n$ (T is in the ith mesh layer $L_{ev,i}$ and suppose $T \subset T'_{(i+1)} \in \mathcal{T}_{i+1}$). Note that the mapping $\mathbf{B}^{(2)}_{v,i}$ in (12) translates $L_{ev,i}$ to $L_{ev,0}$ on $T_{(0)}$, and therefore translates $T'_{(i+1)}$ to a triangle $\hat{T}_{(i+1)} \in \mathcal{T}_1$ in $L_{ev,0}$. Our estimates are based on $T'_{(i+1)}$'s element type. (I) $T'_{(i+1)}$ is an o-element. Based on Algorithm 2.4, T is generated after $n - i - 1$ midpoint refinements of $T'_{(i+1)}$. Thus, the mapping $\mathbf{K} : T \to \hat{T} = \hat{T}_{(i+1)}$ satisfies for $(x, y) \in T$ and $(\hat{x}, \hat{y}) \in \hat{T}$ the same condition as in (20). Following similar calculations as in (21) and (22), we therefore have

$$\|\nabla w\|_{L^2(T)}^2 \leq C \sum_{\ell \in I_T} w_\ell^2 \tag{34}$$

and

$$\|w\|_{L^2(T)}^2 = \int_T w^2 dx dy \geq C 2^{2(i-n)} \kappa_p^{2i} \int_{\hat{T}} \hat{w}^2 d\hat{x} d\hat{y}$$

$$\geq C 2^{2(i-n)} \kappa_p^{2i} \|\hat{w}\|_{L^\infty(\hat{T})}^2 \geq C 2^{2(i-n)} \kappa_p^{2i} \sum_{\ell \in I_T} w_\ell^2. \tag{35}$$

(II) $T'_{(i+1)}$ is a v_e-element. Let $T' = \mathbf{B}_{v,i}^{(2)} T \subset \hat{T} = \hat{T}_{(i+1)} := \mathbf{B}_{v,i}^{(2)} T'_{(i+1)} \in \mathcal{T}_1$. For $(x, y) \in T$, define $(x', y') = \mathbf{B}_{v,i}^{(2)}(x, y)$ and $w'(x', y') = w(x, y)$. Therefore, T' is generated after $n - i - 1$ graded refinements of $\hat{T}_{(i+1)}$ toward the singular vertex with the grading parameter κ_e. Suppose that T' is in the kth ($k < n - i$) layer of the triangulation on the v_e-element $\hat{T}_{(i+1)}$ that is translated from $\mathcal{T}_n$ on $T_{(i+1)}$. Then, by the calculation involved in (21) and (15), we have

$$\|\nabla w\|_{L^2(T)}^2 \leq C \|\nabla w'\|_{L^2(T')}^2 \leq C \sum_{\ell \in I_T} w_\ell^2. \tag{36}$$

Meanwhile, following the scaling argument and by the estimate (17), we have

$$\|w\|_{L^2(T)}^2 = \int_T w^2 dx dy \geq C \kappa_p^{2i} \int_{T'} w'^2 dx' dy' \geq C \kappa_p^{2i} \kappa_e^{2k} 2^{2(k-n+i)} \sum_{\ell \in I_T} w_\ell^2. \tag{37}$$

(III) $T'_{(i+1)}$ is an e-element. We set up the notation similar to that above. Let $T' = \mathbf{B}_{v,i}^{(2)} T \subset \hat{T} = \hat{T}_{(i+1)} := \mathbf{B}_{v,i}^{(2)} T'_{(i+1)} \in \mathcal{T}_1$. For $(x, y) \in T$, define $(x', y') = \mathbf{B}_{v,i}^{(2)}(x, y)$ and $w'(x', y') = w(x, y)$. Therefore, T' is generated after $n - i - 1$ graded refinements of $\hat{T}_{(i+1)}$ toward the singular edge with the grading parameter κ_e. Suppose that T' is in the kth ($k < n - i$) layer of the triangulation on the e-element $\hat{T}_{(i+1)}$ that is translated from $\mathcal{T}_n$ on $T_{(i+1)}$. Then, by the calculation involved in (21) and by the estimate (23), we have

$$\|\nabla w\|_{L^2(T)}^2 \leq C \|\nabla w'\|_{L^2(T')}^2 \leq C(2\kappa_e)^{i-n} \sum_{\ell \in I_T} w_\ell^2 \leq C(2\kappa_e)^{-n} \sum_{\ell \in I_T} w_\ell^2. \tag{38}$$

Meanwhile, following the scaling argument and by the estimate (24), we have

$$\|w\|_{L^2(T)}^2 = \int_T w^2 dx dy = \kappa_p^{2i} \int_{T'} w'^2 dx' dy' \geq C \kappa_p^{2i} 2^{2(k-n+i)} \kappa_e^{2k} \sum_{\ell \in I_T} w_\ell^2. \tag{39}$$

Then, we obtain (29) by summing up the estimates (32), (34), (36), and (38) over all $T \subset D_{ev}$. The estimates (30) and (31) are due to (33), (35), (37), and (39). □

Consequently, we have the estimate on the condition number of the finite element matrix from 2D NoMAC meshes.

Theorem 3.4. *Let $\mathbf{A}$ be the stiffness matrix in (6) associated with the 2D NoMAC mesh $\mathcal{T}_n$ (Algorithm 2.4). Then, for any $w \in S_n$, we have*

$$\mathbf{w}^T \mathbf{w} \leq C 2^{2n} \|\nabla w\|_{L^2(\Omega)}^2, \tag{40}$$

where $\mathbf{w}$ is the coefficient vector of w defined in (7). In addition, the condition number of $\mathbf{A}$ satisfies

$$\text{cond}(\mathbf{A}) \leq C(2\kappa^{-1})^n, \tag{41}$$

where $\kappa = \min_e(\kappa_e, 0.5)$ and the minimum is taken over all the singular edges.

Proof. Recall the regions (D_o, D_v, D_{v_e}, D_e, D_{ev}) and the index sets (I_o, I_v, I_{v_e}, I_e, I_{ev}) from Lemmas 3.1 – 3.3. We shall need the following weighted Poincaré inequality (42). Let $\rho(x, y)$ be the distance from $(x, y) \in \Omega$ to the boundary $\partial\Omega$. Then, by Theorem 8.4 in [27], for any $\sigma \in [0, 1]$, we have

$$\|\nabla w\|_{L^2(\Omega)}^2 \geq C \|\rho^{-\sigma} w\|_{L^2(\Omega)}^2$$

$$\geq C \left(\sum_{T \subset D_o} \|w\|_{L^2(T)}^2 + \sum_{T \subset D_v} \|\rho^{-\sigma} w\|_{L^2(T)}^2 + \sum_{T \subset D_{v_e}} \|\rho^{-\sigma} w\|_{L^2(T)}^2 \right.$$

$$\left. + \sum_{T \subset D_e} \|\rho^{-\sigma} w\|_{L^2(T)}^2 + \sum_{T \subset D_{ev}} \|\rho^{-\sigma} w\|_{L^2(T)}^2 \right). \tag{42}$$

We estimate these terms as follows.

Let $T \in \mathcal{T}_n$ be a triangle in D_v or D_{v_e}. Suppose T is in the ith layer $L_{v,i}$ of an initial triangle with κ_p as the grading parameter toward the singular vertex. Let $\rho_p(x, y)$ be the distance function to the singular vertex. In addition to $\rho \leq \rho_p$, note that $\rho_p \simeq \kappa_p^i$ on $L_{v,i}$ for $i < n$ and $\rho_p \leq C\kappa_p^n$ on $L_{v,n}$. Define $\sigma_p := 1 + \log_{\kappa_p} 2$. It is clear that for $0 < \kappa_p < 0.5$, $\sigma_p \in (0, 1)$. Then, we can pick any $\sigma_p \leq \sigma \leq 1$, and by (17), we have

$$\|\rho^{-\sigma} w\|_{L^2(T)}^2 \geq \|\rho_p^{-\sigma} w\|_{L^2(T)}^2 \geq C 2^{2(i-n)} \kappa_p^{2i} \sum_{\ell \in I_T} \kappa_p^{-2i\sigma} w_\ell^2 \geq C 2^{-2n} \sum_{\ell \in I_T} w_\ell^2.$$

Combining these estimates over all the mesh layers on $D_v \cup D_{v_e}$, we have

$$\sum_{T \subset D_v \cup D_{D_{v_e}}} \|\rho^{-\sigma} w\|_{L^2(T)}^2 \geq C 2^{-2n} \sum_{\ell \in I_v \cup I_{v_e}} w_\ell^2. \tag{43}$$

Then, we consider a triangle $T \in \mathcal{T}_n$ in D_e and suppose T is in the ith layer $L_{e,i}$ of an initial triangle with κ_e as the grading parameter toward the singular edge. By Definition 2.8 for the mesh layers, it can be seen that $\rho \simeq \kappa_e^i$ on $L_{e,i}$ for $i < n$ and $\rho \leq C\kappa_e^n$ on $L_{e,n}$. Define $\sigma_e := 1 + \log_{\kappa_e} 2$. Then, we have $\sigma_e \in (0, 1)$. We can pick any $\sigma_e \leq \sigma \leq 1$, and by (24), we have

$$\|\rho^{-\sigma} w\|_{L^2(T)}^2 \geq C 2^{2(i-n)} \kappa_e^{2i} \sum_{\ell \in I_T} \kappa_e^{-2i\sigma} w_\ell^2 \geq C 2^{-2n} \sum_{\ell \in I_T} w_\ell^2.$$

Combining these estimates over all the mesh layers on D_e, we have

$$\sum_{T \subset D_e} \|\rho^{-\sigma} w\|_{L^2(T)}^2 \geq C 2^{-2n} \sum_{\ell \in I_e} w_\ell^2. \tag{44}$$

Now let $T \in \mathcal{T}_n$ be a triangle in D_{ev}. Suppose T is in the ith layer $L_{ev,i}$ of an initial triangle with κ_p and κ_e as the grading parameters toward the singular vertex and toward the singular edge, respectively. Suppose $T \subset T'_{(i+1)} \in \mathcal{T}_{i+1}$ for $i < n$. Recall the distance function to the singular vertex ρ_p. Then, we have two cases to consider. (I) T is in $L_{ev,n}$ or $T'_{(i+1)}$ is an o-element. Note that $\rho_p \simeq \kappa_p^i$ on $L_{ev,i}$ for $i < n$ and $\rho_p \leq C\kappa_p^n$ on $L_{ev,n}$. Define $\sigma_{ev} := 1 + \log_{\kappa_p} 2$. Picking any $\sigma_{ev} \leq \sigma \leq 1$, by (30), we have

$$\|\rho^{-\sigma} w\|_{L^2(T)}^2 \geq \|\rho_p^{-\sigma} w\|_{L^2(T)}^2 \geq C 2^{2(i-n)} \kappa_p^{2i} \sum_{\ell \in I_T} \kappa_p^{-2i\sigma} w_\ell^2 \geq C 2^{-2n} \sum_{\ell \in I_T} w_\ell^2.$$

(II) $T'_{(i+1)}$ ($i < n$) is a v_e- or e-element. Suppose T is in the kth ($k < n - i$) mesh layer of the graded triangulation on $T'_{(i+1)}$. Then, based on Algorithm 2.4, on this kth layer, $\rho \leq C\kappa_p^i \kappa_e^k$. Recall $\sigma_{ev} = 1 + \log_{\kappa_p} 2$ and the fact $\kappa_p \leq \kappa_e$. Then, for any $\sigma_{ev} \leq \sigma \leq 1$, by (31), we have

$$\|\rho^{-\sigma} w\|_{L^2(T)}^2 \geq C 2^{2(i+k-n)} \kappa_p^{2i} \kappa_e^{2k} \sum_{\ell \in I_T} \kappa_p^{-2i\sigma} \kappa_e^{-2k\sigma} w_\ell^2 \geq C 2^{-2n} \sum_{\ell \in I_T} w_\ell^2.$$

Combining these estimates over all the mesh layers on D_{ev}, we have

$$\sum_{T \subset D_{ev}} \|\rho^{-\sigma} w\|_{L^2(T)}^2 \geq C 2^{-2n} \sum_{\ell \in I_{ev}} w_\ell^2. \tag{45}$$

Recall that for all the singular vertices and singular edges, the grading parameters $\kappa_p, \kappa_e \in (0, 0.5)$. Thus, we can always choose $\sigma \in [0, 1]$ such that $\sigma \geq \max_{v,e}(\sigma_v, \sigma_e, \sigma_{ev})$, where the maximum is taken over all the singular vertices and edges. Therefore, by the estimates in (42) – (45) and by (16), we obtain the estimate (40).

Meanwhile, let $\kappa = \min_e(\kappa_e, 0.5)$, where the minimum is taken over all the singular edges. Following (15), (23), and (29), we have

$$\|\nabla w\|_{L^2(\Omega)}^2 \leq C(2\kappa)^{-n} \mathbf{w}^T \mathbf{w}.$$

Then, by (40) and the estimate above, we derive

$$C 2^{-2n} \mathbf{w}^T \mathbf{w} \leq \mathbf{w}^T \mathbf{A} \mathbf{w} = \|\nabla w\|_{L^2(\Omega)}^2 \leq C(2\kappa)^{-n} \mathbf{w}^T \mathbf{w}.$$

Thus, by (8) and (9), we obtain

$$\text{cond}(\mathbf{A}) \leq C(2\kappa^{-1})^n,$$

which completes the proof. $\quad\square$

Remark 3.5. It is interesting to compare Theorem 3.4 with the classical estimate on condition numbers. According to [12], on a 2D shape regular mesh, the condition number of the finite element stiffness matrix $\mathbf{A}_s$ of equation (1) satisfies

$$\text{cond}(\mathbf{A}_s) \leq CN(1 + |\log(Nh_{min}^2)|), \tag{46}$$

where N is the dimension of the finite element space and h_{min} is the smallest element size. Note that for the finite element method on the 2D NoMAC mesh $\mathcal{T}_n$ (Algorithms 2.2 and 2.4), we have $N \simeq 4^n$. Therefore, the result in Theorem 3.4 implies the following. 1. If $\mathcal{T}_n$ is shape regular (namely, no singular edge is present), we have $\text{cond}(\mathbf{A}) \leq CN$. This is consistent with the estimate (46). Note that the isotropic 2D NoMAC mesh is a special case of the rather general "nondegenerate" mesh considered in [12]. It seems that through our analysis the particular geometric structure of the 2D NoMAC can be exploited to obtain a sharper estimate (without the log term) than that in (46), while the estimate (46) should still be valid for general nondegenerate meshes. 2. If $\mathcal{T}_n$ is anisotropic (with special refinements toward the edge), the upper bound of the condition number involves the edge grading parameter and is larger than the dimension N of the discrete space.

3.2. The 3D case

The estimates of the condition numbers in the 3D case follow a similar path as in the 2D case. For the tetrahedral mesh $\mathcal{T}_n$, we shall first derive estimates on different local sub-regions depending on its relation with the singular vertices and singular edges. Recall that the regions D_o, D_v, D_{v_e}, D_e, and D_{ev} are unions of initial elements in $\mathcal{T}_0$ whose type is indicated via the index of the region.

Lemma 3.6. Let $T \in \mathcal{T}_n$ be a tetrahedron. Let I_o be the set of indices of the nodes in $\mathcal{T}_n$ that lie in $\bar{D}_o$. Similarly, let I_v and I_{v_e} be the sets of indices of the nodes in $\mathcal{T}_n$ that lie in $\bar{D}_v$ and $\bar{D}_{v_e}$, respectively. Then, for $T \subset D_o$, we have

$$\sum_{T \subset D_o} \|\nabla w\|_{L^2(T)}^2 \leq C2^{-n} \sum_{\ell \in I_o} w_\ell^2, \tag{47}$$

$$\sum_{\ell \in I_o} w_\ell^2 \leq C2^{3n} \sum_{T \subset D_o} \|w\|_{L^2(T)}^2. \tag{48}$$

For $T \subset D_v \cup D_{v_e}$, suppose T is in the ith mesh layer (Definition 2.6) on an initial element with κ_p as the grading parameter toward the singular vertex. Let I_T be the set of indices of the nodes in $\bar{T}$. Then, we have

$$\|\nabla w\|_{L^2(T)}^2 \leq C2^{-n}(2\kappa_p)^i \sum_{\ell \in I_T} w_\ell^2, \tag{49}$$

$$\sum_{\ell \in I_T} w_\ell^2 \leq C2^{3(n-i)}\kappa_p^{-3i} \|w\|_{L^2(T)}^2. \tag{50}$$

Proof. Note that the mesh on D_o is quasi-uniform with mesh size $O(2^{-n})$. For each initial tetrahedron in D_o, such midpoint decompositions produce tetrahedra that belong to at most three similarity classes [13]. Let $\hat{T}$ be the reference tetrahedron with vertices $(0, 0, 0)$, $(1, 0, 0)$, $(0, 1, 0)$, and $(0, 0, 1)$. Let $T \in \mathcal{T}_n$ be a tetrahedron in D_o and let $\mathbf{K}: T \to \hat{T}$ be the standard affine mapping. Then, by the scaling argument and the norm equivalence in finite-dimensional spaces, we obtain

$$\sum_{T \subset D_o} \|\nabla w\|_{L^2(T)}^2 = \sum_{T \subset D_o} \int_T (\partial_x w)^2 + (\partial_y w)^2 + (\partial_z w)^2 dx dy dz$$

$$\leq C2^{-n} \sum_{T \subset D_o} \int_{\hat{T}} (\partial_{\hat{x}} \hat{w})^2 + (\partial_{\hat{y}} \hat{w})^2 + (\partial_{\hat{z}} \hat{w})^2 d\hat{x} d\hat{y} d\hat{z}$$

$$\leq C2^{-n} \sum_{T \subset D_o} \|\hat{w}\|_{L^\infty(\hat{T})}^2 \leq C2^{-n} \sum_{\ell \in I_o} w_\ell^2. \tag{51}$$

Meanwhile, by the scaling argument and the norm equivalence in finite-dimensional spaces, we have

$$\sum_{T \subset D_o} \|w\|_{L^2(T)}^2 = \sum_{T \subset D_o} \int_T w^2 dx dy dz \geq C2^{-3n} \sum_{T \subset D_o} \int_{\hat{T}} \hat{w}^2 d\hat{x} d\hat{y} d\hat{z}$$

$$\geq C2^{-3n} \sum_{T \subset D_o} \|\hat{w}\|_{L^\infty(\hat{T})}^2 \geq C2^{-3n} \sum_{\ell \in I_o} w_\ell^2. \tag{52}$$

For a tetrahedron T in D_v or in D_{v_e}, suppose T is in the ith layer of an initial tetrahedron $T_{(0)}$. As in Definition 2.6, let $T_{(i)} \subset T_{(0)}$ be the element in $\mathcal{T}_i$ ($0 \leq i \leq n$) that touches the singular vertex of $T_{(0)}$. Then, if $i = n$, we have $T = T_{(n)}$; if

$i < n$, we have $T \subset T'_{(i+1)} \subset T_{(i)}$, where $T'_{(i+1)} \in \mathcal{T}_{i+1}$ is an o-element. Based on Algorithm 2.4, if $i < n$, T is generated after $n - i - 1$ midpoint refinements of $T'_{(i+1)}$. Recall from Proposition 2.12 that $\mathbf{B}^{(3)}_{v,i}$ maps $T_{(i)}$ to $\hat{T} := T_{(0)}$. Then, the mapping $\mathbf{K} : T \to \hat{T}$ satisfies for $(x, y, z) \in T$ and $(\hat{x}, \hat{y}, \hat{z}) = \mathbf{K}(x, y, z) \in \hat{T}$,

$$\begin{cases} (\partial_x w)^2 + (\partial_y w)^2 + (\partial_z w)^2 \leq C 2^{2(n-i)} \kappa_p^{-2i} \left((\partial_{\hat{x}} \hat{w})^2 + (\partial_{\hat{y}} \hat{w})^2 + (\partial_{\hat{z}} \hat{w})^2 \right), \\ dxdydz \simeq 2^{3(i-n)} \kappa_p^{3i} d\hat{x} d\hat{y} d\hat{z}. \end{cases} \tag{53}$$

Therefore, by (53) and the norm equivalence in finite-dimensional spaces, we derive

$$\begin{aligned} \|\nabla w\|^2_{L^2(T)} &= \int_T (\partial_x w)^2 + (\partial_y w)^2 + (\partial_z w)^2 dxdydz \\ &\leq C 2^{-n} (2\kappa_p)^i \int_{\hat{T}} (\partial_{\hat{x}} \hat{w})^2 + (\partial_{\hat{y}} \hat{w})^2 + (\partial_{\hat{z}} \hat{w})^2 d\hat{x} d\hat{y} d\hat{z} \leq C 2^{-n} (2\kappa_p)^i \|\hat{w}\|^2_{L^\infty(\hat{T})} \\ &\leq C 2^{-n} (2\kappa_p)^i \sum_{\ell \in I_T} w_\ell^2. \end{aligned} \tag{54}$$

Meanwhile, using the scaling argument as in (53) and the norm equivalence in finite-dimensional spaces, we have

$$\begin{aligned} \|w\|^2_{L^2(T)} &= \int_T w^2 dxdydz \geq 2^{3(i-n)} \kappa_p^{3i} \int_{\hat{T}} \hat{w}^2 d\hat{x} d\hat{y} d\hat{z} \\ &\geq C 2^{3(i-n)} \kappa_p^{3i} \|\hat{w}\|^2_{L^\infty(\hat{T})} \geq C 2^{3(i-n)} \kappa_p^{3i} \sum_{\ell \in I_T} w_\ell^2. \end{aligned} \tag{55}$$

Then, we have proved the estimate (47) by (51). The estimates (48) and (50) are due to (52) and (55), respectively. The estimate (49) is due to (54). $\quad \square$

The estimates in the region close to the singular edge read as follows.

Lemma 3.7. *Let $T \in \mathcal{T}_n$ be an tetrahedron in D_e. Let I_e be the set of indices of the nodes in $\mathcal{T}_n$ that lie in $\bar{D}_e$. In addition, suppose T is in the ith mesh layer (Definition 2.8) on an initial e-element with κ_e as the grading parameter toward the singular edge. Let I_T be the set of indices of the nodes in $\bar{T}$. Then, we have*

$$\sum_{T \subset D_e} \|\nabla w\|^2_{L^2(T)} \leq C 2^{-n} \sum_{\ell \in I_e} w_\ell^2, \tag{56}$$

$$\sum_{\ell \in I_T} w_\ell^2 \leq C 2^{3(n-i)} \kappa_e^{-3i} \|w\|^2_{L^2(T)}. \tag{57}$$

Proof. Let $T \subset D_e$ be in the ith layer of an initial e-element $T_{(0)}$. Let $T_{(i)} \in \mathcal{T}_i$ be the tetrahedron such that $T \subset T_{(i)}$. Then, according to Definition 2.8, $T_{(i)}$ is either an e-element or a v_e-element. Based on Algorithm 2.4, if $i = n$, we have $T = T_{(n)}$. If $i < n$, we have $T \subset T'_{(i+1)} \subset T_{(i)}$, where $T'_{(i+1)} \in \mathcal{T}_{i+1}$ is an o-element, and T is generated after $n - i - 1$ midpoint refinements of $T'_{(i+1)}$. We proceed as in the proof of Lemma 3.2 by considering the following two cases.

Case I. $T_{(i)}$ is an e-element in $\mathcal{T}_i$. According to Proposition 2.13, $\mathbf{B}^{(3)}_{e,i}$ maps $T'_{(i+1)}$ ($i < n$) or $T_{(n)}$ ($i = n$) to a reference triangle $\hat{T}$ whose geometry only depends on $T_{(0)}$. Then, the mapping $\mathbf{K} : T \to \hat{T}$ satisfies for $(x, y, z) \in T$ and $(\hat{x}, \hat{y}, \hat{z}) \in \hat{T}$,

$$\begin{cases} (\partial_x w)^2 + (\partial_y w)^2 + (\partial_z w)^2 \leq C 2^{2(n-i)} \kappa_e^{-2i} \left((\partial_{\hat{x}} \hat{w})^2 + (\partial_{\hat{y}} \hat{w})^2 + (\partial_{\hat{z}} \hat{w})^2 \right), \\ dxdydz \simeq 2^{-3n} (2\kappa_e)^{2i} d\hat{x} d\hat{y} d\hat{z}. \end{cases}$$

Let I_T be the set of indices of the nodes in $\bar{T}$. Then, by the scaling argument and the norm equivalence in finite-dimensional spaces, we have

$$\begin{aligned} \|\nabla w\|^2_{L^2(T)} &\leq C \int_{\hat{T}} 2^{2n} (2\kappa_e)^{-2i} \left((\partial_{\hat{x}} \hat{w})^2 + (\partial_{\hat{y}} \hat{w})^2 + (\partial_{\hat{z}} \hat{w})^2 \right) 2^{-3n} (2\kappa_e)^{2i} d\hat{x} d\hat{y} d\hat{z} \\ &\leq C 2^{-n} \|\hat{w}\|^2_{L^\infty(\hat{T})} \leq C 2^{-n} \sum_{\ell \in I_T} w_\ell^2. \end{aligned} \tag{58}$$

Meanwhile, using the scaling argument and the norm equivalence in finite dimensional spaces, we have

$$\|w\|^2_{L^2(T)} = \int_T w^2 dxdydz \geq C2^{-3n}(2\kappa_e)^{2i} \int_{\hat{T}} \hat{w}^2 d\hat{x}d\hat{y}d\hat{z}$$

$$\geq C2^{-3n}(2\kappa_e)^{2i}\|\hat{w}\|^2_{L^\infty(\hat{T})} \geq C2^{-3n}(2\kappa_e)^{2i} \sum_{\ell \in I_T} w^2_\ell. \tag{59}$$

Case II. $T_{(i)}$ is a v_e-element in $\mathcal{T}_i$. Let $T_{(k)} \in \mathcal{T}_k$, $1 \leq k \leq i$, be the v_e-element, such that $T_{(i)} \subset T_{(k)}$ and $T_{(k)}$'s parent element $T_{(k-1)} \in \mathcal{T}_{k-1}$ is an e-element. According to Proposition 2.13, $\mathbf{B}^{(3)}_{i,k}$ maps $T'_{(i+1)}$ ($i < n$) or $T_{(n)}$ ($i = n$) to a reference triangle $\hat{T}$ whose geometry only depends on $T_{(0)}$. Then, the mapping $\mathbf{K} : T \to \hat{T}$ satisfies for $(x, y, z) \in T$ and $(\hat{x}, \hat{y}, \hat{z}) \in \hat{T}$,

$$\begin{cases} (\partial_x w)^2 + (\partial_y w)^2 + (\partial_z w)^2 \leq C2^{2(n-i)}\kappa_e^{-2i} \left((\partial_{\hat{x}}\hat{w})^2 + (\partial_{\hat{y}}\hat{w})^2 + (\partial_{\hat{z}}\hat{w})^2\right), \\ dxdydz \simeq 2^{-3n}(2\kappa_e)^{3i-k}d\hat{x}d\hat{y}d\hat{z}. \end{cases}$$

Let I_T be the set of indices of the nodes in $\hat{T}$. Then, we have

$$\|\nabla w\|^2_{L^2(T)} \leq C\int_{\hat{T}} 2^{2n-2i}\kappa_e^{-2i}\left((\partial_{\hat{x}}\hat{w})^2 + (\partial_{\hat{y}}\hat{w})^2 + (\partial_{\hat{z}}\hat{w})^2\right)2^{-3n}(2\kappa_e)^{3i-k}d\hat{x}d\hat{y}d\hat{z}$$

$$\leq C2^{-n}(2\kappa_e)^{i-k}\|\hat{w}\|^2_{L^\infty(\hat{T})} \leq C2^{-n}(2\kappa_e)^{i-k}\sum_{\ell \in I_T} w^2_\ell. \tag{60}$$

Meanwhile, using the scaling argument and the norm equivalence in finite-dimensional spaces, we have

$$\|w\|^2_{L^2(T)} = \int_T w^2 dxdydz \geq C2^{-3n}(2\kappa_e)^{3i-k} \int_{\hat{T}} \hat{w}^2 d\hat{x}d\hat{y}d\hat{z}$$

$$\geq C2^{-3n}(2\kappa_e)^{3i-k}\|\hat{w}\|^2_{L^\infty(\hat{T})} \geq C2^{-3n}(2\kappa_e)^{3i-k}\sum_{\ell \in I_T} w^2_\ell. \tag{61}$$

Recall $k \leq i \leq n$ and $\kappa_e < 0.5$. Then, we obtain (56) by summing up the estimates (58) and (60) over all $T \subset D_e$. The estimate (57) is due to (59) and (61). $\square$

Then, we present the estimates in the region that close to the singular vertex and single edge in 3D.

Lemma 3.8. *Let $T \in \mathcal{T}_n$ be a tetrahedron in D_{ev}. Let I_{ev} be the set of indices of the nodes in $\mathcal{T}_n$ that lie in $\bar{D}_{ev}$. Let I_T be the set of indices of the nodes in $\bar{T}$. Then, we have*

$$\sum_{T \subset D_{ev}} \|\nabla w\|^2_{L^2(T)} \leq C2^{-n} \sum_{\ell \in I_{ev}} w^2_\ell. \tag{62}$$

In addition, suppose T is in the ith mesh layer (Definition 2.10) of an initial ev-element, with κ_p and κ_e as the grading parameter for the singular vertex and for the singular edge, respectively. For $i < n$, let $T'_{(i+1)} \in \mathcal{T}_{i+1}$ be the tetrahedron that contains T. Then, if $T'_{(i+1)}$ is an o-element or if $i = n$, we have

$$\sum_{\ell \in I_T} w^2_\ell \leq C2^{3(n-i)}\kappa_p^{-3i}\|w\|^2_{L^2(T)}. \tag{63}$$

If $T'_{(i+1)}$ ($i < n$) is a v_e- or e-element, suppose T is in the kth ($k < n - i$) layer (Definitions 2.6 and 2.8) of the graded triangulation on $T'_{(i+1)}$ toward the singular vertex or toward the singular edge. Then, we have

$$\sum_{\ell \in I_T} w^2_\ell \leq C2^{3(n-i-k)}\kappa_p^{-3i}\kappa_e^{-3k}\|w\|^2_{L^2(T)}. \tag{64}$$

Proof. For a tetrahedron T in D_{ev}, suppose $T \subset T_{(0)}$, where $T_{(0)}$ is an initial ev-element in $\mathcal{T}_0$ with singular vertex v and e. Therefore, T is either in the ith mesh layer $L_{ev,i}$ if $i < n$ and $T \subset T'_{(i+1)}$ for some $T'_{(i+1)} \in \mathcal{T}_{i+1}$; or $T = T_{(n)} \subset L_{ev,n}$.

We first consider the case when $i = n$, namely $T = T_{(n)}$. Then, the dilation $\mathbf{B}^{(3)}_{v,n}$ in (12) maps T to $\hat{T} = T_{(0)}$. Therefore, using the same arguments as in Lemma 3.6 (see also (49) and (50)), we have

$$\|\nabla w\|^2_{L^2(T)} \leq C\kappa_p^n \sum_{\ell \in I_T} w^2_\ell, \tag{65}$$

$$\sum_{\ell \in I_T} w^2_\ell \leq C\kappa_p^{-3n}\|w\|^2_{L^2(T)}. \tag{66}$$

We now consider the case when $i < n$ (T is in the ith mesh layer $L_{ev,i}$ and suppose $T \subset T'_{(i+1)} \in \mathcal{T}_{i+1}$). Then, the mapping $\mathbf{B}^{(3)}_{v,i}$ in (12) translates $L_{v,i}$ to $L_{v,0}$ on $T_{(0)}$, and therefore translates $T'_{(i+1)}$ to a tetrahedron $\hat{T}'_{(i+1)} \in \mathcal{T}_1$ in $L_{v,0}$. We formulate the estimate based on $T'_{(i+1)}$'s element type. (I) $T'_{(i+1)}$ is an o-element. Based on Algorithm 2.4, T is generated after $n-i-1$ midpoint refinements of $T'_{(i+1)}$. Thus, the mapping $\mathbf{K}: T \to \hat{T} = \hat{T}'_{(i+1)}$ satisfies for $(x, y, z) \in T$ and $(\hat{x}, \hat{y}, \hat{z}) \in \hat{T}$ the same condition as in (53). Following similar calculations as in (54) and (55), we therefore have

$$\|\nabla w\|^2_{L^2(T)} \le C 2^{-n} (2\kappa_p)^i \sum_{\ell \in I_T} w^2_\ell, \tag{67}$$

$$\|w\|^2_{L^2(T)} \ge C 2^{3(i-n)} \kappa_p^{3i} \sum_{\ell \in I_T} w^2_\ell. \tag{68}$$

(II) $T'_{(i+1)}$ is a v_e-element. Let $T' = \mathbf{B}^{(3)}_{v,i} T \subset \hat{T} = \hat{T}'_{(i+1)} \in \mathcal{T}_1$. For $(x, y, z) \in T$, define $(x', y', z') = \mathbf{B}^{(3)}_{v,i}(x, y, z)$ and $w'(x', y', z') = w(x, y, z)$. Therefore, T' is generated after $n-i-1$ graded refinements of $\hat{T}'_{(i+1)}$ toward the singular vertex with the grading parameter κ_e. Suppose that T' is in the kth ($k < n-i$) layer of the triangulation on the v_e-element $\hat{T}'_{(i+1)}$ that is translated from $\mathcal{T}_n$ on $T'_{(i+1)}$. Then, by the calculation involved in (54) and (49), we have

$$\|\nabla w\|^2_{L^2(T)} \le C 2^{-n} (2\kappa_p)^i \|\nabla w'\|^2_{L^2(T')} \le C 2^{-n} (2\kappa_p)^i 2^{i-n} (2\kappa_e)^k \sum_{\ell \in I_T} w^2_\ell. \tag{69}$$

Meanwhile, following the scaling argument, the estimate (50), we have

$$\|w\|^2_{L^2(T)} = \int_T w^2 dx dy dz = \kappa_p^{3i} \int_{T'} w'^2 dx' dy' dz' \ge C \kappa_p^{3i} 2^{3(k-n+i)} \kappa_e^{3k} \sum_{\ell \in I_T} w^2_\ell. \tag{70}$$

(III) $T'_{(i+1)}$ is an e-element. Let $T' = \mathbf{B}^{(3)}_{v,i} T \subset \hat{T} = \hat{T}'_{(i+1)} \in \mathcal{T}_1$. For $(x, y, z) \in T$, define $(x', y', z') = \mathbf{B}^{(3)}_{v,i}(x, y, z)$ and $w'(x', y', z') = w(x, y, z)$. Therefore, T' is generated after $n-i-1$ graded refinements of $\hat{T}'_{(i+1)}$ toward the singular edge with the grading parameter κ_e. Suppose that T' is in the kth ($k < n-i$) layer of the triangulation on the e-element $\hat{T}'_{(i+1)}$ that is translated from $\mathcal{T}_n$ on $T'_{(i+1)}$. Then, by the calculation involved in (54) and the estimates (58) and (60), we have

$$\|\nabla w\|^2_{L^2(T)} \le C 2^{-n} (2\kappa_p)^i \|\nabla w'\|^2_{L^2(T')} \le C 2^{2(i-n)} \kappa_p^i \sum_{\ell \in I_T} w^2_\ell. \tag{71}$$

Meanwhile, following the scaling argument, the estimate (50), and the estimate (57), we have

$$\|w\|^2_{L^2(T)} = \int_T w^2 dx dy dz = \kappa_p^{3i} \int_{T'} w'^2 dx' dy' dz' \ge C \kappa_p^{3i} 2^{3(k-n+i)} \kappa_e^{3k} \sum_{\ell \in I_T} w^2_\ell. \tag{72}$$

Then, we obtain (62) by summing up the estimates (65), (67), (69), and (71) over all $T \subset D_{ev}$. The estimates (63) and (64) are due to (66), (68), (70), and (72). □

We now have the estimates on the condition number of the finite element method on $\mathcal{T}_n$.

Theorem 3.9. *Let $\mathbf{A}$ be the stiffness matrix in (6) associated with the 3D NoMAC mesh $\mathcal{T}_n$ (Algorithm 2.4). Let $\kappa = \min_{v,e}(\kappa_v, \kappa_e, 0.5)$, where the minimum is taken over all the singular vertices and singular edges. Then, for any $w \in S_n$, we have*

$$\mathbf{w}^T \mathbf{w} \le C \|\nabla w\|^2_{L^2(\Omega)} \left(\begin{cases} 2^{3n} & \text{for } \kappa \ge 0.125 \\ \kappa^{-n} & \text{for } 0 < \kappa < 0.125 \end{cases} \right), \tag{73}$$

where $\mathbf{w}$ is the coefficient vector of w defined in (7). In addition, the condition number of $\mathbf{A}$ satisfies

$$\text{cond}(\mathbf{A}) \le \begin{cases} C 2^{2n} & \text{for } \kappa \ge 0.125 \\ C(2\kappa)^{-n} & \text{for } 0 < \kappa < 0.125. \end{cases} \tag{74}$$

Proof. Recall the regions $(D_o, D_v, D_{v_e}, D_e, D_{ev})$ and the index sets $(I_o, I_v, I_{v_e}, I_e, I_{ev})$ from Lemmas 3.6 – 3.8. Let $\rho(x, y, z)$ be the distance from $(x, y, z) \in \Omega$ to the boundary $\partial\Omega$. Then, by Theorem 8.4 in [27], we have the weighted Poincaré inequality

$$\|\nabla w\|_{L^2(\Omega)}^2 \geq C\|\rho^{-1}w\|_{L^2(\Omega)}^2$$

$$\geq C\Big(\sum_{T \subset D_o} \|w\|_{L^2(T)}^2 + \sum_{T \subset D_v} \|\rho^{-1}w\|_{L^2(T)}^2 + \sum_{T \subset D_{v_e}} \|\rho^{-1}w\|_{L^2(T)}^2$$

$$+ \sum_{T \subset D_e} \|\rho^{-1}w\|_{L^2(T)}^2 + \sum_{T \subset D_{ev}} \|\rho^{-1}w\|_{L^2(T)}^2 \Big). \tag{75}$$

We shall estimate these terms in the corresponding regions.

Let $T \in \mathcal{T}_n$ be a tetrahedron in D_v or in D_{v_e}. Suppose T is in the ith layer $L_{v,i}$ of an initial tetrahedron with κ_p as the grading parameter to the singular vertex. Note that $\rho \simeq \kappa_p^i$ on $L_{v,i}$ for $i < n$ and $\rho \leq C\kappa_p^n$ on $L_{v,n}$. Then, by (50), we have

$$\|\rho^{-1}w\|_{L^2(T)}^2 \geq C2^{-3n}2^{3i}\kappa_p^{(3-2)i} \sum_{\ell \in I_T} w_\ell^2 \geq C2^{-3n}2^{3i}\kappa_p^i \sum_{\ell \in I_T} w_\ell^2. \tag{76}$$

Consider a tetrahedron $T \in \mathcal{T}_n$ in D_e and suppose T is in the ith layer $L_{e,i}$ of an initial tetrahedron with κ_e as the grading parameter to the singular edge. Note that $\rho \simeq \kappa_e^i$ on $L_{e,i}$ for $i < n$ and $\rho \leq C\kappa_e^n$ on $L_{e,n}$. Then by (57), we have

$$\|\rho^{-1}w\|_{L^2(T)}^2 \geq C2^{-3n}2^{3i}\kappa_e^{(3-2)i} \sum_{\ell \in I_T} w_\ell^2 \geq C2^{-3n}2^{3i}\kappa_e^i \sum_{\ell \in I_T} w_\ell^2. \tag{77}$$

Now let $T \in \mathcal{T}_n$ be a tetrahedron in D_{ev}. Suppose T is in the ith layer $L_{ev,i}$ of an initial tetrahedron with κ_p and κ_e as the parameters to the singular vertex and the singular edge. Suppose $T \subset T'_{(i+1)} \in \mathcal{T}_{i+1}$ if $i < n$. Let ρ_p be the distance function to the singular vertex. It is clear that $\rho \leq \rho_p$. Then, we have two cases to consider. (I) T is in $L_{ev,n}$ or $T'_{(i+1)}$ is an o-element. Note that $\rho_p \simeq \kappa_p^i$ on $L_{ev,i}$ for $i < n$ and $\rho_p \leq C\kappa_p^n$ on $L_{ev,n}$. Then, by (63), we have

$$\|\rho^{-1}w\|_{L^2(T)}^2 \geq \|\rho_p^{-1}w\|_{L^2(T)}^2 \geq C2^{-3n}2^{3i}\kappa_p^{(3-2)i} \sum_{\ell \in I_T} w_\ell^2 \geq C2^{-3n}2^{3i}\kappa_p^i \sum_{\ell \in I_T} w_\ell^2. \tag{78}$$

(II) $T'_{(i+1)}$ ($i < n$) is a v_e- or e-element. Suppose T is in the kth ($k < n-i$) mesh layer of the graded triangulation on $T'_{(i+1)}$. Then, on this kth layer, $\rho \leq C\kappa_p^i\kappa_e^k$. Recall $\kappa_p \leq \kappa_e$. Then, by (64), we have

$$\|\rho^{-1}w\|_{L^2(T)}^2 \geq C2^{-3n}2^{3(i+k)}\kappa_p^{(3-2)i}\kappa_e^{(3-2)k} \sum_{\ell \in I_T} w_\ell^2 \geq C2^{-3n}2^{3(i+k)}\kappa_p^i\kappa_e^k \sum_{\ell \in I_T} w_\ell^2. \tag{79}$$

Recall the definition of κ_p in (11). Let N be the dimension of the finite element space. Then, for $\kappa = \min_{v,e}(\kappa_v, \kappa_e, 0.5)$, where the minimum is taken over all the singular vertices and singular edges, according to the estimates (48) and (75) – (79), we obtain

$$\|\nabla w\|_{L^2(\Omega)}^2 \geq C \sum_{T \in \mathcal{T}_n} \|\rho^{-1}w\|_{L^2(T)}^2 \geq C \sum_{1 \leq \ell \leq N} w_\ell^2 \Big(\begin{cases} 2^{-3n} & \text{for } \kappa \geq 0.125 \\ \kappa^n & \text{for } 0 < \kappa < 0.125 \end{cases} \Big)$$

$$\geq C\mathbf{w}^T\mathbf{w} \Big(\begin{cases} 2^{-3n} & \text{for } \kappa \geq 0.125 \\ \kappa^n & \text{for } 0 < \kappa < 0.125 \end{cases} \Big).$$

Therefore, we have proved the desired estimate in (73). In addition, by (47), (49), (56), and (62), we have

$$\|\nabla w\|_{L^2(\Omega)}^2 \leq C2^{-n} \sum_{1 \leq \ell \leq N} w_\ell^2 \leq C2^{-n}\mathbf{w}^T\mathbf{w}. \tag{80}$$

Then, the estimate (74) on the condition number is an immediate consequence of (8) – (10), (80), and (73). □

Remark 3.10. It is clear that the estimate on the condition number from the 3D NoMAC mesh (Theorem 3.9) is different than the 2D counterpart (Theorem 3.4). In the 3D estimate, the grading parameters to the singular vertex and to the singular edge play a similar role in the bounds while only the edge parameter was involved in the 2D case. Note that the dimension of the finite element space satisfies $N \simeq 8^n$ on the 3D NoMAC mesh $\mathcal{T}_n$. Recall from [12] the following result for a preconditioned stiffness matrix $\mathbf{A}_s$ on 3D shape regular meshes,

$$\text{cond}(\mathbf{A}_s) \leq CN^{2/3}.$$

Therefore, for mild grading NoMAC meshes in 3D ($\kappa \geq 0.125$), the estimate (74) resembles that for the preconditioned stiffness matrix on shape regular meshes. The threshold $\kappa = 0.125$ is the by-product of the estimates in (78) and (79), where an additional factor 2^{3i} or $2^{3(i+k)}$ helps balance the effect from κ until $\kappa < 0.125$. The estimates in Theorems 3.4 and 3.9 recover the classical estimates on condition numbers when the usual midpoint decomposition is used in the mesh refinement. It can be seen by letting h be the mesh size of $\mathcal{T}_n$ after n refinements. Then $h \simeq 2^{-n}$. For both the 2D and 3D cases, since $\kappa = 0.5$ for the midpoint decomposition, the estimates in Theorems 3.4 and 3.9 become $\text{cond}(\mathbf{A}) \leq Ch^{-2}$.

Table 1
Condition numbers on NoMAC meshes: 2D vertex refinements in the L-shaped domain (Fig. 5).

n	$\kappa_v = 0.5$		$\kappa_v = 0.4$		$\kappa_v = 0.3$		$\kappa_v = 0.2$		$\kappa_v = 0.1$	
	cond	r_n	cond	r_n	cond	r_n	cond	r_n	cond	r_n
3	5.18E1	4.22	4.87E1	4.57	4.73E1	4.73	4.73E1	4.70	8.97E1	5.75
4	2.11E2	4.06	2.06E2	4.22	2.01E2	4.24	2.03E2	4.28	4.01E2	4.47
5	8.47E2	4.02	8.36E2	4.07	8.15E2	4.07	8.29E2	4.09	1.65E3	4.12
6	3.40E3	4.01	3.36E3	4.02	3.28E3	4.02	3.34E3	4.03	6.66E3	4.03

Table 2
Condition numbers on NoMAC meshes: 2D edge refinements in the square domain (Fig. 6).

n	$\kappa_e = 0.5$		$\kappa_e = 0.4$		$\kappa_e = 0.3$		$\kappa_e = 0.2$		$\kappa_e = 0.1$	
	cond	r_n	cond	r_n	cond	r_n	cond	r_n	cond	r_n
3	5.15E1	4.07	5.49E1	4.51	8.61E1	6.09	2.11E2	9.18	1.30E3	18.3
4	2.07E2	4.02	2.69E2	4.90	5.65E2	6.57	2.08E3	9.84	2.56E4	19.7
5	8.30E2	4.00	1.34E3	4.98	3.77E3	6.67	2.07E4	9.97	5.10E5	19.9
6	3.32E3	4.00	6.69E3	5.00	2.52E4	6.69	2.07E5	9.99	1.02E7	20.0

4. Numerical illustrations

In this section, we report numerical test results to verify the estimates on condition numbers (Theorem 3.4 and Theorem 3.9). In particular, these are the condition numbers of the stiffness matrix (6) from equation (1) on 2D and 3D NoMAC meshes. We focus on the growth rate of the condition numbers between consecutive refinements in relation to different types of grading parameters. For a given domain Ω, we use the same notation: denoting by $\mathcal{T}_0$ and $\mathcal{T}_n$ the initial triangulation and the triangulation after n graded refinements (Algorithm 2.4), respectively. Recall the finite element space S_n in (4) associated with the mesh $\mathcal{T}_n$ and its dimension $N = \dim(S_n)$. Note that $N \simeq 4^n$ (2D) and $N \simeq 8^n$ (3D).

The first set of tests is for meshes on 2D domains: the L-shaped domain and the square domain. On the L-shaped domain (Fig. 5), graded meshes are generated toward the re-entrant vertex. These meshes are isotropic and effectively approximating the corner singularity in the solution. In Table 1, we list the condition numbers of the stiffness matrices from different values of the grading parameter κ_v. The growth rate r_n is the ratio of the condition numbers from two consecutive mesh levels. Namely, let $\mathbf{A}_{n-1}$ and $\mathbf{A}_n$ ($n \geq 1$) be the stiffness matrices on $\mathcal{T}_{n-1}$ and $\mathcal{T}_n$, respectively. Then,

$$r_n := \frac{\text{cond}(\mathbf{A}_n)}{\text{cond}(\mathbf{A}_{n-1})}.$$

Recall that $\kappa_v = 0.5$ corresponds to the midpoint decomposition. It is clear from the table that for different values of κ_v, although the actual condition numbers are different, the growth rate is the same, converging to 4. This is consistent with the result in Theorem 3.4 and in [12]. Namely, the condition numbers grow by a factor of 4 on such graded meshes for each refinement.

On the square domain (Fig. 6), we test the NoMAC mesh with special refinements toward an edge with the grading parameter κ_e. The test results are listed in Table 2. For $\kappa_e < 0.5$, the triangles close to the edge e can be very thin with the maximum angle approaching π as $n \to \infty$. Therefore, the meshes are highly anisotropic and lack of the maximum angle condition. According to Theorem 3.4, the condition numbers grow by a factor of $2\kappa_e^{-1}$ for each refinement of these meshes. We see a strong agreement between the numerical growth rates in Table 2 and this theoretical prediction.

The second set of tests is for meshes on three typical 3D domains: the tetrahedral domain, the prism domain, and the Fichera corner domain. The NoMAC mesh has shown its effectiveness in approximating 3D singular solutions [30,32]. We here use these domains to test the condition numbers corresponding to different types of refinements.

On the tetrahedral domain (Fig. 7), we implement the graded meshes toward a vertex with the grading parameter κ_v. These meshes are isotropic and become smaller in size near the vertex v to improve the approximation to the possible vertex singularity. On the prism domain (Fig. 8), we implement the graded meshes toward the singular edge e with the grading parameter κ_e. These meshes are anisotropic when $\kappa_e < 0.5$ and do not maintain the maximum angle condition. Such anisotropic property in the mesh is consistent with the anisotropic behavior of the possible singular solution near the edge. Based on Theorem 3.9, in both cases, the condition numbers grow for each refinement by a factor that is determined by the estimate (74). Namely, when the grading parameter is greater than or equal to 0.125, the growth rate should be 4, which is the same rate as for the midpoint refinement. When the grading parameter is less than 0.125, the condition numbers are expected to grow by a factor of $(2\kappa)^{-1}$, where $\kappa = \kappa_v$ for the tetrahedral domain and $\kappa = \kappa_e$ for the prism domain. In Table 3 and Table 4, we list the condition numbers for these two domains. These test results verify our theory: for $\kappa \geq 0.125$, the growth rates are 4, while for $\kappa = 0.1, 0.08$ and 0.05, the growth rates follow another theoretical estimate $(2\kappa)^{-1}$.

On the domain with the Fichera corner (Fig. 9), the graded elements are concentrating toward the three singular edges e_1, e_2, and e_3, and also toward the singular vertex v. According to Algorithm 2.4, we choose the same grading parameter $\kappa :=$

Table 3
Condition numbers on NoMAC meshes: 3D vertex refinements in the tetrahedral domain (Fig. 7).

n	$\kappa_v = 0.5$		$\kappa_v = 0.4$		$\kappa_v = 0.3$		$\kappa_v = 0.2$	
	cond	r_n	cond	r_n	cond	r_n	cond	r_n
3	5.69E0	5.69	5.27E0	5.27	5.53E0	5.53	6.77E0	6.77
4	2.48E1	4.37	2.41E1	4.57	2.60E1	4.70	3.12E1	4.61
5	1.02E2	4.09	1.05E2	4.37	1.15E2	4.41	1.32E2	4.24
6	4.09E2	4.02	4.32E2	4.11	4.73E2	4.12	5.41E2	4.08
7	1.64E3	4.01	1.74E3	4.03	1.91E3	4.03	2.18E3	4.02

n	$\kappa_v = 0.1$		$\kappa_v = 0.08$		$\kappa_v = 0.05$	
	cond	r_n	cond	r_n	cond	r_n
3	1.16E1	11.6	1.48E1	14.8	2.66E1	26.6
4	7.79E1	6.73	1.17E2	7.96	3.40E2	12.8
5	4.20E2	5.39	7.90E2	6.72	3.61E3	10.6
6	2.15E3	5.12	5.05E3	6.39	3.68E4	10.2
7	1.08E4	5.03	3.17E4	6.29	3.70E5	10.1

Table 4
Condition numbers on NoMAC meshes: 3D edge refinements in the prism domain (Fig. 8).

n	$\kappa_e = 0.5$		$\kappa_e = 0.4$		$\kappa_e = 0.3$		$\kappa_e = 0.2$	
	cond	r_n	cond	r_n	cond	r_n	cond	r_n
3	2.75E1	4.49	3.28E1	4.82	4.27E1	5.05	6.39E1	5.71
4	1.15E2	4.18	1.44E2	4.37	1.90E2	4.44	2.98E2	4.66
5	4.66E2	4.05	5.95E2	4.15	7.96E2	4.20	1.26E3	4.25
6	1.87E3	4.02	2.41E3	4.06	3.25E3	4.08	5.17E3	4.09
7	7.50E3	4.01	9.69E3	4.02	1.31E4	4.02	2.08E4	4.03

n	$\kappa_e = 0.1$		$\kappa_e = 0.08$		$\kappa_e = 0.05$	
	cond	r_n	cond	r_n	cond	r_n
3	1.39E2	7.36	1.91E2	8.37	4.38E2	12.3
4	7.30E2	5.28	1.10E3	5.78	4.40E3	10.1
5	3.37E3	4.61	6.75E3	6.11	4.51E4	10.3
6	1.46E4	4.33	4.25E4	6.30	4.57E5	10.1
7	6.90E4	4.73	2.66E5	6.27	4.58E6	10.0

Table 5
Condition numbers on NoMAC meshes: 3D vertex and edge refinements ($\kappa = \kappa_v = \kappa_{e_i}$, $1 \le i \le 3$) in the domain with the Fichera corner (Fig. 9).

n	$\kappa = 0.5$		$\kappa = 0.4$		$\kappa = 0.3$		$\kappa = 0.2$		$\kappa = 0.1$	
	cond	r_n	cond	r_n	cond	r_n	cond	r_n	cond	r_n
3	6.20E1	4.38	8.75E1	4.73	1.45E2	5.42	2.85E2	6.55	1.58E3	11.4
4	2.57E2	4.14	3.83E2	4.38	6.76E2	4.67	1.73E3	6.05	1.49E4	9.43
5	1.04E3	4.05	1.60E3	4.18	2.88E3	4.26	8.61E3	4.99	9.68E4	6.51
6	4.18E3	4.02	6.50E3	4.07	1.17E4	4.07	3.79E4	4.41	5.29E5	5.46
7	1.67E4	4.00	2.62E4	4.02	4.73E4	4.02	1.57E5	4.13	2.72E6	5.14

$\kappa_v = \kappa_{e_i}$ ($1 \le i \le 3$) for the singular vertex and edges to simplify the implementation. Note that we need many tetrahedra in the initial mesh due to the complex geometry of the domain. Therefore, with the same number of refinements, the size of the stiffness matrix in this test is much larger than those in the other two tests on 3D domains. The test results are displayed in Table 5, which also validate the estimate in Theorem 3.9: for $\kappa \ge 0.125$, the growth rate is 4 and for $\kappa < 0.125$, the growth rate is bounded by $(2\kappa)^{-1}$.

In the tests above, the stiffness matrices are defined as in (6) on NoMAC meshes. According to Algorithm 2.4, if the grading refinement is only for the vertex of the domain (see Fig. 7 for a 3D example), the resulting meshes are isotropic and shape regular [30]. In this case, a simple diagonal preconditioner [12] will result in a scaled stiffness matrix whose condition number is bounded by the estimate in (2). In 3D, this means the condition numbers of the scaled stiffness matrix grow by a factor of 4 for consecutive graded refinements regardless of the grading parameter. We display the condition numbers in this case in Table 6 for the readers' reference. Comparing the results in Table 6 and in Table 3, it is clear that the diagonal preconditioner can improve the conditioning of the FEMs. We point out, however, that this preconditioning

Table 6
Condition numbers of the scaled stiffness matrix on NoMAC meshes: 3D vertex refinements in the tetrahedral domain (Fig. 7).

n	$\kappa_v = 0.5$		$\kappa_v = 0.4$		$\kappa_v = 0.3$		$\kappa_v = 0.2$	
	cond	r_n	cond	r_n	cond	r_n	cond	r_n
3	5.19E0	5.19	5.07E0	5.07	5.54E0	5.54	7.30E0	7.30
4	2.26E1	4.36	2.21E1	4.38	2.47E1	4.46	3.45E1	4.72
5	9.26E1	4.09	9.14E1	4.12	1.03E2	4.15	1.46E2	4.24
6	3.72E2	4.02	3.69E2	4.04	4.15E2	4.05	5.97E2	4.07
7	1.49E3	4.00	1.48E3	4.02	1.67E3	4.01	2.40E3	4.02

n	$\kappa_v = 0.1$		$\kappa_v = 0.08$		$\kappa_v = 0.05$	
	cond	r_n	cond	r_n	cond	r_n
3	1.54E1	15.4	2.02E1	20.2	3.61E1	36.1
4	7.98E1	5.20	1.06E2	5.25	1.94E2	5.37
5	3.43E2	4.30	4.55E2	4.29	8.24E2	4.26
6	1.40E3	4.09	1.86E3	4.09	3.36E3	4.08
7	5.65E3	4.02	7.47E3	4.02	1.35E4	4.02

technique is not well defined for anisotropic meshes toward singular edges. Further investigation is needed to develop good preconditioners for the finite element equations on anisotropic NoMAC meshes.

References

[1] T. Apel, Anisotropic Finite Elements: Local Estimates and Applications, Advances in Numerical Mathematics, B. G. Teubner, Stuttgart, 1999.
[2] T. Apel, B. Heinrich, Mesh refinement and windowing near edges for some elliptic problem, SIAM J. Numer. Anal. 31 (3) (1994) 695–708.
[3] T. Apel, S. Nicaise, The finite element method with anisotropic mesh grading for elliptic problems in domains with corners and edges, Math. Methods Appl. Sci. 21 (6) (1998) 519–549.
[4] T. Apel, S. Nicaise, J. Schöberl, Finite element methods with anisotropic meshes near edges, in: Finite Element Methods, Jyväskylä, 2000, in: GAKUTO Internat. Ser. Math. Sci. Appl., vol. 15, Gakkōtosho, Tokyo, 2001, pp. 1–8.
[5] T. Apel, A.-M. Sändig, J. Whiteman, Graded mesh refinement and error estimates for finite element solutions of elliptic boundary value problems in non-smooth domains, Math. Methods Appl. Sci. 19 (1) (1996) 63–85.
[6] T. Apel, J. Schöberl, Multigrid methods for anisotropic edge refinement, SIAM J. Numer. Anal. 40 (5) (2002) 1993–2006 (electronic).
[7] I. Babuška, A.K. Aziz, On the angle condition in the finite element method, SIAM J. Numer. Anal. 13 (2) (1976) 214–226.
[8] I. Babuška, R.B. Kellogg, J. Pitkäranta, Direct and inverse error estimates for finite elements with mesh refinements, Numer. Math. 33 (4) (1979) 447–471.
[9] C. Bacuta, H. Li, V. Nistor, Anisotropic graded meshes and quasi-optimal rates of convergence for the FEM on polyhedral domains in 3D, in: Proceedings of European Congress on Computational Methods in Applied Sciences and Engineering, in: CCOMAS 2012 - European Congress on Computational Methods in Applied Sciences and Engineering, e-Book Full Papers, 2012, pp. 9003–9014.
[10] C. Băcuţă, V. Nistor, L.T. Zikatanov, Improving the rate of convergence of 'high order finite elements' on polygons and domains with cusps, Numer. Math. 100 (2) (2005) 165–184.
[11] C. Bacuta, V. Nistor, L.T. Zikatanov, Improving the rate of convergence of high-order finite elements on polyhedra. II. Mesh refinements and interpolation, Numer. Funct. Anal. Optim. 28 (7–8) (2007) 775–824.
[12] R.E. Bank, L.R. Scott, On the conditioning of finite element equations with highly refined meshes, SIAM J. Numer. Anal. 26 (6) (1989) 1383–1394.
[13] J. Bey, Tetrahedral grid refinement, Computing 55 (4) (1995) 355–378.
[14] S.C. Brenner, J. Cui, L.-Y. Sung, Multigrid methods for the symmetric interior penalty method on graded meshes, Numer. Linear Algebra Appl. 16 (6) (2009) 481–501.
[15] S.C. Brenner, L.R. Scott, The Mathematical Theory of Finite Element Methods, second edition, Texts in Applied Mathematics, vol. 15, Springer-Verlag, New York, 2002.
[16] P. Ciarlet, The Finite Element Method for Elliptic Problems, Studies in Mathematics and Its Applications., vol. 4, North-Holland, Amsterdam, 1978.
[17] M. Dauge, Elliptic Boundary Value Problems on Corner Domains, Lecture Notes in Mathematics, vol. 1341, Springer-Verlag, Berlin, 1988.
[18] A. Demlow, A posteriori error estimation and adaptivity, Lecture Notes.
[19] A. Demlow, R. Stevenson, Convergence and quasi-optimality of an adaptive finite element method for controlling L_2 errors, Numer. Math. 117 (2) (2011) 185–218.
[20] L. Formaggia, S. Perotto, New anisotropic a priori error estimates, Numer. Math. 89 (4) (2001) 641–667.
[21] L. Formaggia, S. Perotto, Anisotropic error estimates for elliptic problems, Numer. Math. 94 (1) (2003) 67–92.
[22] R. Fritzsch, Optimale Finite-Elemente-Approximationen für Funktionen mit Singularitäten, Thesis (Ph.D.)–TU Dresden, 1990.
[23] E.H. Georgoulis, E. Hall, P. Houston, Discontinuous Galerkin methods for advection-diffusion-reaction problems on anisotropically refined meshes, SIAM J. Sci. Comput. 30 (1) (2007/2008) 246–271.
[24] P. Grisvard, Elliptic Problems in Nonsmooth Domains, Monographs and Studies in Mathematics, vol. 24, Pitman (Advanced Publishing Program), Boston, MA, 1985.
[25] E. Hunsicker, H. Li, V. Nistor, V. Uski, Analysis of Schrödinger operators with inverse square potentials II: FEM and approximation of eigenfunctions in the periodic case, Numer. Methods Partial Differ. Equ. 30 (4) (2014) 1130–1151.
[26] M. Křížek, On the maximum angle condition for linear tetrahedral elements, SIAM J. Numer. Anal. 29 (2) (1992) 513–520.
[27] A. Kufner, Weighted Sobolev Spaces, John Wiley & Sons, 1984.
[28] G. Kunert, A posteriori error estimation for convection dominated problems on anisotropic meshes, Math. Methods Appl. Sci. 26 (7) (2003) 589–617.
[29] H. Li, A-priori analysis and the finite element method for a class of degenerate elliptic equations, Math. Comput. 78 (2009) 713–737.
[30] H. Li, An anisotropic finite element method on polyhedral domains: interpolation error analysis, Math. Comput. 87 (312) (2018) 1567–1600.
[31] H. Li, A. Mazzucato, V. Nistor, Analysis of the finite element method for transmission/mixed boundary value problems on general polygonal domains, Electron. Trans. Numer. Anal. 37 (2010) 41–69.

[32] H. Li, S. Nicaise, Regularity and a priori error analysis on anisotropic meshes of a Dirichlet problem in polyhedral domains, Numer. Math. 139 (1) (2018) 47–92.

[33] H. Li, S. Nicaise, A priori analysis of an anisotropic finite element method for elliptic equations in polyhedral domains, Comput. Methods Appl. Math. (2020).

[34] H. Li, Q. Zhang, Optimal quadrilateral finite elements on polygonal domains, J. Sci. Comput. 70 (1) (2017) 60–84.

[35] J. Lubuma, S. Nicaise, Dirichlet problems in polyhedral domains. II. Approximation by FEM and BEM, J. Comput. Appl. Math. 61 (1) (1995) 13–27.

[36] P. Morin, R. Nochetto, K. Siebert, Convergence of adaptive finite element methods, SIAM Rev. 44 (4) (2002) 631–658 (electronic) (2003). Revised reprint of "Data oscillation and convergence of adaptive FEM", SIAM J. Numer. Anal. 38 (2) (2000) 466–488 (electronic); MR1770058 (2001g:65157).

[37] D. Schötzau, Ch. Schwab, T.P. Wihler, *hp*-dGFEM for second-order elliptic problems in polyhedra I: stability on geometric meshes, SIAM J. Numer. Anal. 51 (3) (2013) 1610–1633.

[38] D. Schötzau, Ch. Schwab, T.P. Wihler, *hp*-DGFEM for second order elliptic problems in polyhedra II: exponential convergence, SIAM J. Numer. Anal. 51 (4) (2013) 2005–2035.

[39] D. Schötzau, Ch. Schwab, T.P. Wihler, *hp*-dGFEM for second-order mixed elliptic problems in polyhedra, Math. Comput. 85 (299) (2016) 1051–1083.

[40] U. Trottenberg, C.W. Oosterlee, A. Schüller, Multigrid, Academic Press Inc., San Diego, CA, 2001. With contributions by A. Brandt, P. Oswald and K. Stüben.

[41] J. Xu, T. Tang (Eds.), Adaptive Computations: Theory and Algorithms, Science Press, 2007.